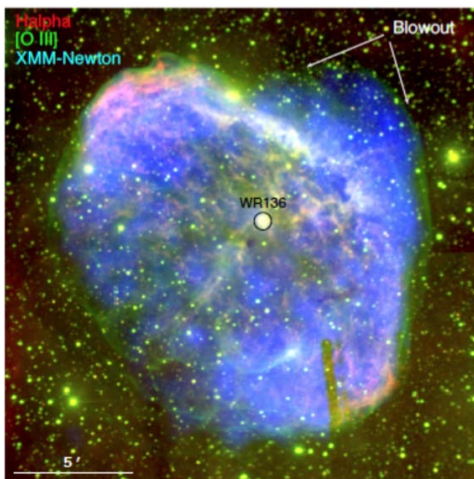


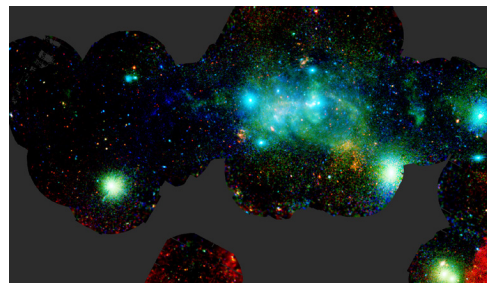
XMM-Newton 2016 Senior Review Proposal

XMM-Newton Guest Observer Facility, Guest Observer Funding, and the US RGS Hardware Team

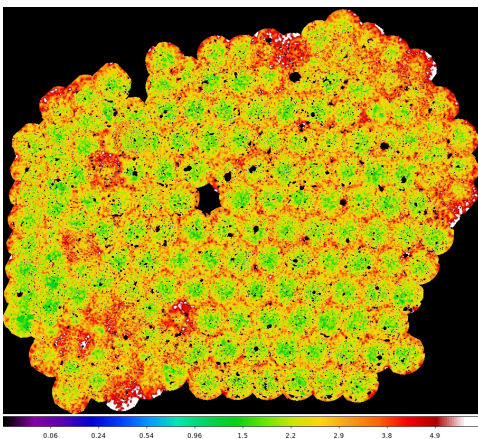
Prepared by: S. L. Snowden (NASA Project Scientist),
the US XMM-Newton Users Group (C. Sarazin, Chair;
Members: L. Brenneman, M. Gagne, J. Halpern, J. Irwin, and B. Williams)
the US Mission Scientist (R. Mushotzky),
and staffs of the US RGS Team and US XMM-Newton GOF



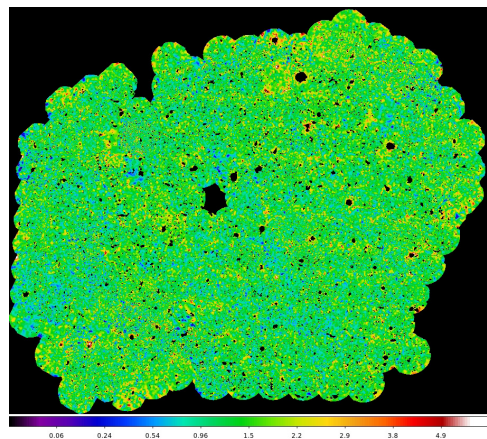
Composite image of the NGC 6888 bubble around Wolf-Rayet star WR 136 (Toalá et al. 2015c, see §1.4.5, Fig. 13). The X-ray data were processed using XMM-ESAS.



False color mosaic image of all XMM observations within 1° of Sgr A (Ponti et al. 2015, see §1.4.4, Fig. 10).



XMM XXL-South VLP before ESAS processing (see §1.4.10).



XXL-South region after ESAS background modeling and subtraction demonstrating the improvement in the utility of the data.

1.4 XMM-Newton Science

While §1.4 focuses on the *XMM* science of the last two years, we also consider where new observations may lead by examining the 21 LP/VLPs proposals accepted in AO-14/15 in “Future Science” boxes. Nine of these proposals have US PIs, and a further 9 have US Co-Is. As such, they will provide US astronomers with immediate access to a wealth of astrophysical data.

The future science of *XMM* will be considerably enhanced by the availability of the well-calibrated and extensive EPIC Serendipitous Source Catalog (SSC) Data Release 5 and associated data products (3XMM-DR5), EPIC Slew Survey Source Catalog (SSSC), OM Catalog (OMCat, produced by the US GOF), and OM Serendipitous Source Survey (OM SUSS, produced by ESA). These databases are invaluable resources for archival research, and they will continue to grow in value as deeper, wide-field multiwavelength surveys become available for follow-up. The science proposed for *XMM* is often based on past observations, both where objects are re-observed with deeper exposures after preliminary survey observations, and where the target is expected to have long-term temporal variations.

Continual improvements in calibration and the advent of new software allow measurements, for example, of the soft X-ray background, Galactic plane emission, and measurement of the mass profiles of clusters. The continued development of the *XMM* Science Analysis System (SAS) has made analysis easier and more robust as well as providing new automatic data products, easing the analysis of the large and complex data sets.

Demonstrating the wealth of *XMM* discoveries in the last two years requires focusing on a small representative fraction of the results. The following is just a sample of what has been accomplished since the last Senior Review. One final note, the references have been color coded where red indicates a US lead author, purple indicates a foreign lead author with US coauthors, and blue indicates no US authors.

1.4.1 Active Galactic Nuclei (AGN)

XMM has provided a revolutionary and unique view of AGNs over the last 15 years, and this science continues to be a cornerstone of the mission’s portfolio. *XMM*’s superior effective area

enables it to collect spectra with higher signal-to-noise ratios in a given time than any other current X-ray observatory, and its orbit allows for long, continuous observations (~2 d). Combined, these two properties make *XMM* the ideal choice for deep exposures of AGNs, which can vary in flux by up to an order of magnitude in a matter of hours. Further, the simultaneous data collected by the EPIC, RGS, and OM instruments allow astronomers to examine the properties of the absorbing gas/outflowing wind, continuum, distant and inner disk reflection and soft excess self-consistently. In the past two years, *XMM* has also been utilized in tandem with multiple other observatories such as *Chandra*, *HST*, *NuSTAR*, and *INTEGRAL* to obtain simultaneous, broad-band data over the full X-ray range and beyond.

Relativistic Reflection and Black Hole Spin:

The co-evolution of a SMBH with its host galaxy through cosmic time is encoded in its spin. An established method to measure the spins of black holes is via the study of relativistic reflection features from the inner accretion disk. While a broad profile of the Fe K α emission line is frequently found in the X-ray spectra of typical active galaxies, the situation is unclear in the case of narrow line Seyfert 1 (NLS1) galaxies, an extreme subset that are generally thought to harbor less massive black holes with higher accretion rates. [Liu et al. \(2015\)](#) investigated the ensemble properties of the Fe K α line in NLS1s by stacking the X-ray spectra of 51 NLS1s observed with *XMM*. The composite X-ray spectrum reveals a prominent, broad emission feature over 4–7 keV, characteristic of the broad Fe K α line (**Fig. 4**). In addition, there are indications for possible narrow (unresolved) lines, either in emission or absorption, corresponding to Fe xxvi or Fe xxv, respectively. There are tentative indications for low or intermediate values of the average spins of the black holes ($a < 0.84$), as inferred from the profile of the composite broad line (**Fig. 4**).

Owing to their greater distances, there has hitherto been no significant detection of relativistic reflection features in a moderate-redshift quasar. [Reis et al. \(2014\)](#) use archival *Chandra* and *XMM* data together with a new, deep *Chandra* observation of a gravitationally lensed quasar at $z=0.658$ to detect a broad Fe K line from a luminous high redshift quasar for the first time. The spectrum constrains the origin of the emission to within $3 r_g$ from the black hole, implying a spin parameter $a > 0.66$ at the 5σ level. The high spin is indicative of growth via coherent accretion and suggests that black hole growth between $0.5 < z < 1$ occurs principally by coherent rather than chaotic accretion episodes.

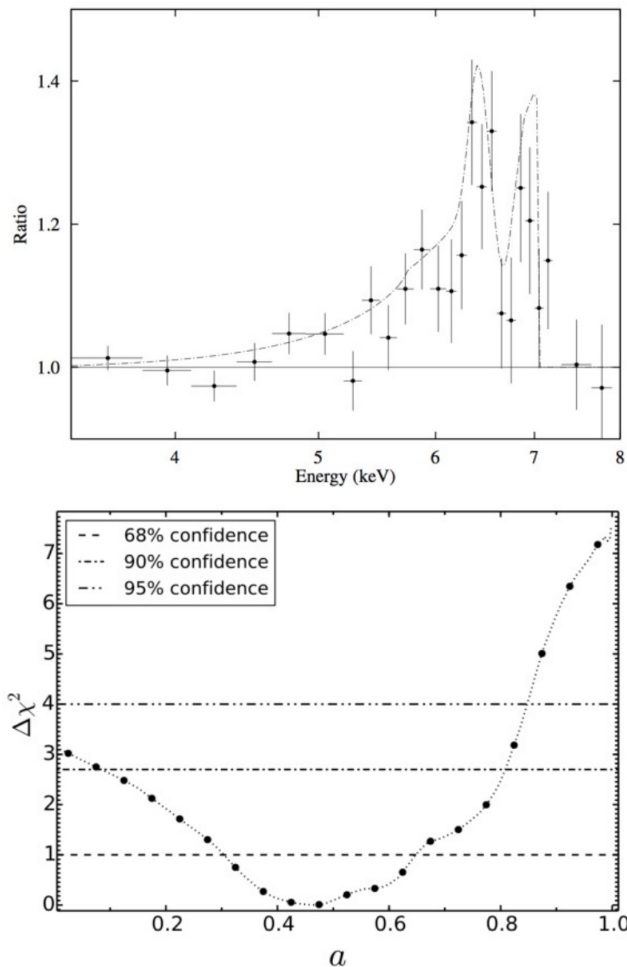


Figure 4. Top: Residual broad Fe K α feature remaining in emission in the stacked NLS1 spectra of Liu et al. (2015) after the continuum power-law is modeled out. Note the additional presence of an ionized H-like emission line at ~ 6.97 keV. Bottom: Parameter space of the black hole spin in the stacked NLS1 spectra of Liu et al. (2015), indicating that a moderate-to-low spin value is preferred in the spectral fit.

Fe K Reverberation Time Lags: Reverberation time lags occur due to light travel time delays between changes in the direct coronal emission and corresponding variations in its reflection from the accretion flow. High-frequency Fe K α lags represent a model-independent confirmation of the interpretation of broad Fe K α lines as signatures of relativistic reflection from a compact reflector close to the black hole. This picture was first indicated by XMM for NGC 4151 (Zoghbi et al. 2012), and has been further supported by the first detections of reverberation lags with the NuSTAR hard X-ray observatory used simultaneously with XMM in NGC 1365 and MCG-5-23-16 (Zoghbi et al. 2014; Kara et al. 2014), among other AGNs. The shape of the Fe K α line changes with timescale (or temporal frequency) in the observation of MCG-5-23-16: at

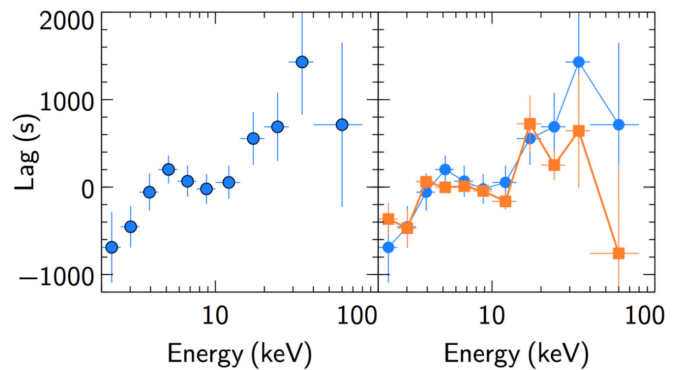


Figure 5. Lag-energy spectra for MCG-5-23-16 using NuSTAR light curves (Zoghbi et al. 2014). Left: Lag-energy spectra for lags averaged over a wide frequency band covering 6×10^{-6} – 6×10^{-4} Hz. Right: Lag-energy spectra at two frequency bands. Blue circles are for the same frequency band as the left panel. The orange squares are for frequencies 3×10^{-5} – 6×10^{-4} Hz. The central frequencies for the two bins are 6×10^{-5} Hz (blue circles) and 10^{-4} Hz (orange squares), respectively.

long timescales, both the blue and red wings of the line are seen, whereas at short timescales, only the red wing is seen. This demonstrates that emission from the innermost disk is responsible for the red wing of the broad Fe K α line, implying that it can be used as a diagnostic for measuring the black hole’s spin. Zoghbi et al. (2014) also report the discovery of a time delay between energies > 10 keV and the continuum seen in the NuSTAR data. These lags are most likely due to reverberation in the reflection Compton hump, and the matching lags strongly imply an origin of this feature in the same reflection processes that creates the broad Fe K α emission line (Fig. 5).

Absorption in the Central Engines of Active Galaxies: The evolution of galaxies is connected to the growth of SMBHs in their centers. During the quasar phase, these AGNs peak in luminosity as matter falls onto the black hole, and radiation-driven winds can transfer most of this energy back to the host galaxy. Over five different epochs from 2013–2014, Nardini et al. (2015) detected P Cygni features in the Fe K emission from the luminous quasar PDS 456 using contemporaneous XMM and NuSTAR observations, allowing strong constraints on the energy, covering fraction, velocity and mass loss of its persistent wind. The wind is expelled at relativistic speeds from the inner accretion disk, creating a broadened Fe K α emission component (Fig. 6). The wide aperture of this outflow suggests an effective coupling with the ambient gas. The outflow has a kinetic power larger than 10^{46} erg s $^{-1}$, which is enough to provide the feedback required by models of black hole and host galaxy co-evolution.

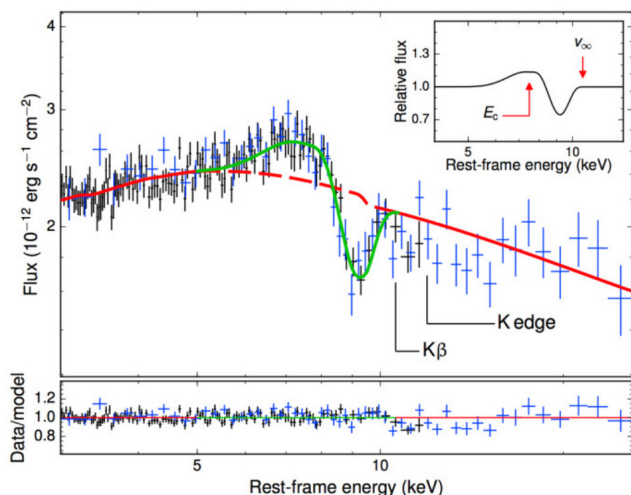


Figure 6. Emission and absorption residuals characterizing the Fe K band of PDS 456 (Nardini et al. 2015) by means of a self-consistent P-Cygni profile from a spherically symmetric outflow (green curve). The inset contains a graphical explanation of the key parameters of this model: the characteristic energy corresponding to the onset of the absorption component, and the wind terminal velocity $v_{\infty} = 0.35 \pm 0.02c$, which can be regarded as a measure of the actual outflowing speed of the gas. The bottom panel shows the ratio between the data and the best-fit model. The residual structures above 10 keV are due to the $K\beta$ and K edge absorption features from Fe XXVI.

Recent X-ray observations show absorbing winds with velocities up to mildly-relativistic values of the order of $v \sim 0.1c$ in a limited sample of 6 broad-line radio galaxies. They are observed as blue-shifted Fe xxv-xxvi K-shell absorption lines, similar to the ultra-fast outflows (UFOs) reported in Seyferts and quasars. Tombesi et al. (2014) extended the search for such Fe K absorption lines to a larger sample of 26 radio-loud AGNs observed with XMM and Suzaku. Combining the results of this analysis with those in the literature, UFOs are detected in $>27\%$ of the sources. However, correcting for the number of spectra with insufficient S/N, the authors estimate that the incidence of UFOs in this sample of radio-loud AGNs is likely in the range $f = (50 \pm 20)\%$. Photo-ionization modeling of the absorption lines with XSTAR reveals that the observed outflow velocities are broadly distributed between $\sim 1000 \text{ km s}^{-1}$ and $\sim 0.4c$, with mean and median values of $v_{out} \sim 0.133c$ and $v_{out} \sim 0.117c$, respectively. The material is highly ionized, with an average ionization parameter of $\log \xi \sim 4.5 \text{ erg cm s}^{-1}$, and the column densities are $>10^{22} \text{ cm}^{-2}$. Overall, these characteristics are consistent with the presence of complex accretion disk winds in a significant fraction of radio-loud AGNs and demonstrate that the presence of

Future AGN Research

XMM observations will continue to capitalize on performing simultaneous observations with other missions, including NuSTAR, HST, Swift, and Astro-H. In AO-14/15, XMM accepted 6 LP/VLP proposals in the field of AGN research including: XMM joint observations with HST, NuSTAR, Swift, and ground-based optical to map out the ionized wind outflow of the highly-accreting AGN NGC 7469; using X-ray relativistic reverberation to map out the inner structure of the AGN in NGC 4151; using XMM to determine the bolometric luminosity and Eddington ratio for about 700 quasars out to $z \sim 4$ with accurate masses from reverberation mapping to determine the cosmic history of accretion; XMM will perform dynamic reverberation observations of the NLS1 galaxy IRAS13224-3809, which shows strong iron-K and L broad lines and high-frequency soft X-ray time lags indicating reflection from the innermost regions about a rapidly spinning black hole; mapping with XMM and NuSTAR of the X-ray reprocessor in NGC 3227, which has rapid X-ray variability, a negative lag, variable Fe K emission and variable absorption; and finally, building on the COSMOS survey, XMM will survey the XMM-LSS field to a depth of 50 ks to detect thousands of AGNs and hundreds of clusters, and will study the growth of SMBHs and galaxies within the context of large scale structure.

relativistic jets does not preclude the existence of winds, in accordance with several theoretical models. Assuming a steady wind, Tombesi et al. infer an estimate of the minimum covering fraction of $C = \Omega/4\pi \sim 0.3-0.7$. This value is comparable to that of UFOs and warm absorbers in radio-quiet AGNs, suggesting that the jet-related radio-quiet/radio-loud AGN dichotomy might not hold for AGN winds.

Multi-Wavelength Observations & Surveys: Heavily obscured, Compton-thick (CT; $N_H > 10^{24} \text{ cm}^{-2}$) AGNs may represent an important phase in AGN/galaxy co-evolution and are expected to provide a significant contribution to the cosmic X-ray background (CXB). Through X-ray spectral analysis, Lanzuisi et al. (2014) selected 39 heavily obscured AGNs ($N_H > 3 \times 10^{23} \text{ cm}^{-2}$) in the 2 deg² XMM-COSMOS survey and were able to confirm that 10 of these are Compton thick and span a large range of redshift and luminosity. The results indicate that highly obscured sources tend to have significantly smaller black hole masses and higher Eddington ratios with respect to unobscured ones. The specific star formation rate of highly obscured sources is consistent with the one observed on the

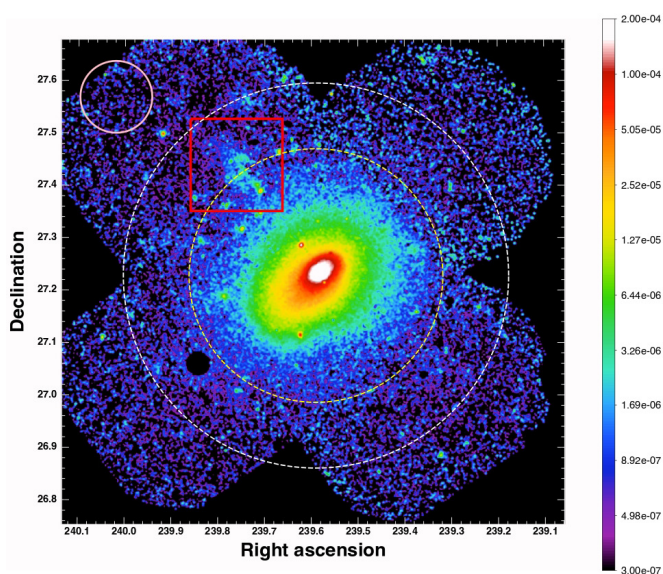


Figure 7. XMM EPIC image of Abell 2142 illustrating the extent of the 800 kpc long structure (red square to the northeast of the main cluster) discovered by [Eckert et al. \(2014\)](#). The inner and outer dotted circles represent $R500$ and $R200$, respectively.

main sequence of star forming galaxies at all redshifts. Exploiting the high-resolution *HST* images available, these highly obscured sources also have a significantly larger merger fraction with respect to other X-ray selected samples of AGNs.

1.4.2 Galaxy Clusters & the Dark Universe

Clusters of Galaxies: Advances in understanding cluster assembly were accomplished with several deep XMM observations of merging activity. [Eckert et al. \(2014\)](#) discovered an X-ray structure >800 kpc in extent in the outskirts of the massive galaxy cluster Abell 2142 associated with a concentration of galaxies, the longest X-ray tail detected to date (**Fig. 7**). The long survival time of this low-entropy structure in the hot halo of Abell 2142 suggests that the infalling material can eventually settle within the core of the main cluster. More subtle signs of cluster assembly can also be revealed by slight asymmetries in the X-ray emission of clusters. [Guennou et al. \(2014\)](#) subtracted symmetric radial profiles from the X-ray emission from 32 clusters in the redshift range $0.4 < z < 0.9$ observed with XMM and found substructure in a substantial fraction of them. For those clusters for which substructure was also indicated based on dynamical studies of the constituent galaxies, it was concluded that 5–15% of the mass of the cluster is included in these substructures. This is in agreement with the percentage of substructure predicted by Lambda Cold Dark Matter (Λ CDM) simulations at $z=0$, suggesting little to no evolution in the amount of substructure in clusters out to a redshift of nearly one.

XMM has aided in the refining of cluster and group X-ray scaling relations, which in turn improves our understanding of these objects as cosmological probes. By taking into account intracluster stars, [Gonzalez et al. \(2013\)](#) found a steeper dependence for the stellar mass fraction of clusters and groups on mass ($f_* \propto M_{500}^{-0.45 \pm 0.04}$) than in previous studies that ignored intracluster stars in the calculation of f_* . They also found the baryon fraction is not independent of halo mass (instead finding $f_b \propto M_{500}^{0.16 \pm 0.04}$) in contrast to previous studies. Recent work has also found that groups of galaxies appear to follow different scaling relations than clusters for a growing number of properties. [Kettula et al. \(2015\)](#) combined X-ray and weak lensing data to conclude that galaxy groups are more luminous and hotter for their mass than clusters, indicated by steepening in the $M-L_X$ and $M-T_X$ scaling relations at low masses. Such a steepening in the $M-L_X$ relation on group mass scales was confirmed with XMM data analyzed by [Lovisari et al. \(2015\)](#).

Dark Matter and the Nature of Gravity: One of the most intriguing controversies over the last several years in all of astrophysics has unfolded thanks to XMM observations of galaxy clusters. The discovery of an unidentified X-ray emission line at 3.57 keV in the stacked spectra of 73 galaxy clusters observed with XMM (**Fig. 8**, [Bulbul et al. 2014](#)), has spurred debate that the line represents long-sought-after evidence for the nature of dark matter. The suggestion is that this line is produced by the decay of 7.1 keV “sterile” neutrinos (right-handed helicity neutrinos). Sterile neutrinos can mix with active neutrinos and decay, producing two photons at an energy equal to roughly half the sterile neutrino’s mass and a very light normal neutrino. Although the predicted rest mass of the sterile neutrino (and thus the X-ray line energy) depends upon which extension to the Standard Model is assumed, other physical constraints suggest that sterile neutrino decay will produce a line in the 0.5–100 keV range. The largest signal is expected from objects with the largest dark matter concentrations, clusters of galaxies, or the centers of nearby galaxies, which are common targets of X-ray observatories. With its large grasp (see **Fig. 1**), XMM is the best instrument for such a search, and no fewer than five searches using archival XMM data have been reported in the last year.

Confirmation of such an X-ray emission line in the spectrum of M31 and the Perseus Galaxy Cluster by [Boyarsky et al. \(2014\)](#) has spawned dozens of theoretical papers attempting to describe the details of such dark matter decay. Indeed, [Bulbul](#)

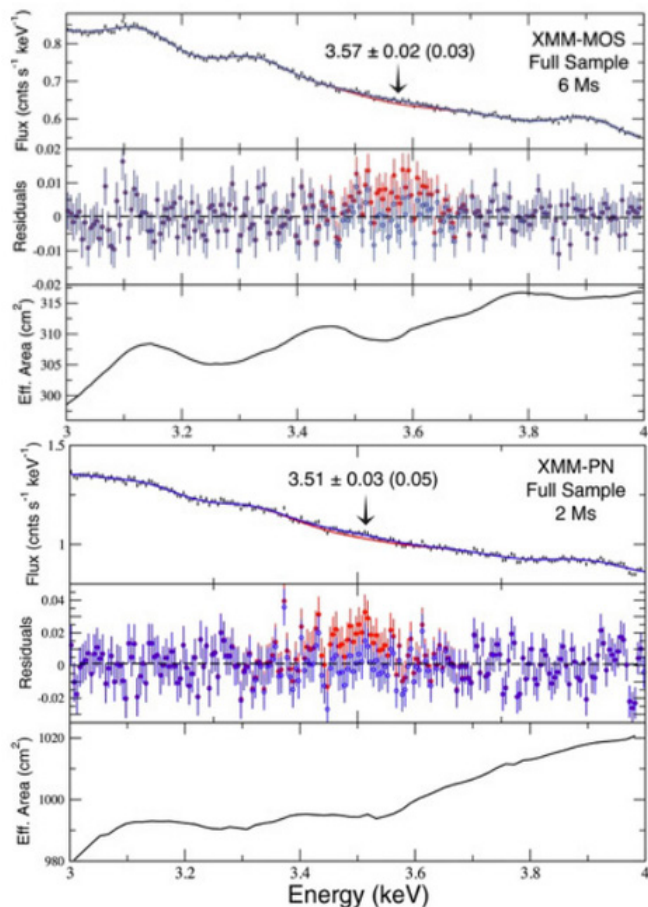


Figure 8. Stacked XMM MOS and PN (left and right, respectively) spectra of 73 clusters in the sample of [Bulbul et al. \(2014\)](#). Red represents the model/residuals without the addition of a Gaussian line at 3.57 keV, while blue represents those quantities after the addition of a Gaussian line at 3.57 keV.

[et al. \(2014\)](#) and [Boyarsky et al. \(2014\)](#) are among the top six highest cited non-*Planck* papers of 2014 in all of astrophysics. [Boyarsky et al. \(2015\)](#) followed up these results with a detection of a 3.53 keV line in the spectrum of the Galactic center.

However, subsequent results have called into question the statistical significance and interpretation of the 3.53–3.57 keV emission line. [Jeltema & Profumo \(2015\)](#) found no evidence of such an emission line in a reanalysis of the XMM data of M31, but did find evidence for excess line emission in the Tycho supernova remnant, which naturally should not show evidence of significant dark matter decay. They suggested that K XVIII lines at 3.48 and 3.52 keV could account for the line detection in cluster spectra. Alternatively, [Gu et al. \(2015\)](#) argue that the 3.5 keV feature is due to a S XVI charge-exchange line. The failure to detect the line in the stacked XMM spectra of dwarf spheroidals ([Malyshev et al. 2014](#)) and groups and galaxies ([Anderson et al. 2015](#)) at the expected level

Future Cluster Research

Given the exciting nature of a potential dark matter decay X-ray emission line at 3.57 keV found by [Bulbul et al. \(2014\)](#), [Boyarsky et al. \(2014\)](#), and [Boyarsky et al. \(2015\)](#) in the spectra of galaxy clusters, M31, and the Galactic Center, a pressing goal of the astronomical community will be to utilize the large collecting area of XMM to fully understand its nature. While the line was detected individually in the very bright Perseus Cluster, stacking of spectra from many clusters was necessary to detect the line in other clusters. Deeper X-ray observations of the best candidates other than Perseus, with a variety of gas temperatures and expected sterile neutrino decay line strengths is the crucial next step in identifying the origin of the emission line and its likelihood of it resulting from dark matter annihilation.

Six LP/VLP proposals were accepted in AO-14/15 for galaxy clusters, large scale structure, and dark Universe research, including: a project to determine the masses of a complete, X-ray selected sample of ~400 clusters, the Extremely Expanded Highest X-ray FLUX Galaxy Cluster Sample (eeHIFLUGCS); searching for the 3.5 keV line in the Draco dwarf spheroidal galaxy; obtaining very deep spectra of the blazar 1ES 1553+113 to finally detect with confidence or decisively limit the baryon content of the WHIM, thought to be primary reservoir of baryons in the Universe, and determine the chemical composition and thermodynamic state of the WHIM; determining the X-ray properties and pressure, entropy, and mass profiles of a complete sample of *Planck*-selected massive clusters in the redshift range of $0.7 < z < 0.9$; finally, XMM will survey the XMM-LSS field to a depth of 50 ks to detect hundreds of clusters, and will study large scale structure in this region.

given the mixing angle of sterile neutrinos predicted by the [Bulbul et al. \(2014\)](#) result has further clouded the issue.

X-ray clusters are also providing a novel means of testing the chameleon gravity model, which hypothesizes that a fifth force of nature comparable in strength to gravity is coupled to matter via a scalar field, possibly providing an explanation for the accelerated expansion of the Universe. While chameleon gravity would affect the measurement of the hot gas properties (X-ray surface brightness and temperature, as well as Sunyaev-Zel'dovich, S-Z, profiles), it would not affect weak lensing mass measurements. Using the stacked X-ray properties of 58 higher redshift clusters observed

with *XMM*, [Wilcox et al. \(2015\)](#) constrained the parameters of chameleon gravity to exclude the need for a fifth force, and hope to extend and strengthen this claim using hundreds of clusters from the Dark Energy Survey.

1.4.3 Galaxies

For the study of galaxies, *XMM*'s strength is its ability to detect extended faint and/or soft emission. [Mitsuishi et al. \(2013\)](#) studied the starburst driven outflow of NGC 253, showing that the abundance pattern in the halo matched that of the disk emission, and that of the base of the wind. They further showed that the energetics of the halo are consistent with being produced by the starburst, and constrained the outflow velocity using the halo temperature gradient.

XMM has been used very successfully to study galactic disks. As part of a larger multi-wavelength study, [Ducci et al. \(2014\)](#) determined the parameters of the diffuse emission in the interacting/starburst galaxy NGC 1512. Also of note is a multi-wavelength study of IRAS 08339+6517, a bright starburst galaxy at ~ 80 Mpc with strong Ly α emission that may be an analog of the strong Ly α emitters at $z=4$. It is of note because the X-ray data were extracted from an archival observation of the star π^1 UMa! The ever-expanding archive allows for the study of many interesting background objects.

Because X-ray charge exchange emission is expected in almost any astrophysical situation where ionized gas encounters colder material, the contribution of charge-exchange emission in the interstellar medium (ISM) in galaxies is of high interest in constraining galactic winds. RGS observations of M82 ([Zhang et al. 2014b](#)) using sophisticated new analysis tools show that the observed spectrum is consistent with a mixture of direct plasma emission and charge-exchange emission. This analysis provided a more refined measure of temperatures and abundances, and a direct measure of the cool gas mass loading in the superwind.

Spiral Galaxies and their Halos: One of the prime questions concerning spiral galaxies is the location and composition of the “missing baryons.” It has been assumed that many of the missing baryons are in the form of a hot halo. The difficulty of determining the scale of the Galaxy’s hot halo, and the difficulty in detecting halos around other spiral galaxies, have left this question unsettled. However, following a similar detection in NGC 1961, [Dai et al. \(2012\)](#), observing UGC 12591 (the fastest rotating spiral) with *XMM*, show that the hot halo contains only 30% of the expected baryons. Given a similar result for the Milky Way (MW, [Miller](#)

& [Bregman 2013](#), see below), *XMM* observations strongly suggest that the missing baryons are not in hot Galactic halos.

Even if halos do not contain the keys to the missing baryon problem, they are interesting in themselves. Halos can be formed by either infall, or by galactic fountains, and it is not clear which mechanism dominates. Thus, halos may either contain a large amount of low-metallicity material (essential for most chemosynthesis models), or can record the star-formation history in enriched material. Starburst galaxies are expected to represent the metal-rich extreme, but even here the evidence is equivocal. *XMM* observations by [Hodges-Kluck & Bregman \(2013\)](#) of the edge-on NGC 891 reveal either a low-metallicity single temperature component spectrum or a solar metallicity two-temperature component spectrum. On the basis of cooling rate and scale height arguments, they favor the low-metallicity case, but the evidence is uncertain. Conversely, [Mitsuishi et al. \(2013\)](#) studying NGC 253 with a combination of *XMM* and *Suzaku* data found the halo to have the same α -enhanced abundances as the superwind.

[Bogdán et al. \(2013\)](#) detected the coronae of two massive spiral galaxies without starbursts, and used these observations to test structure formation simulations ([Bogdán et al. 2015](#)). For both of these coronae, they found temperatures of $kT \sim 0.6$ keV, abundances of $Z \sim 0.12 Z_{\odot}$, masses of $M_{\text{gas}} \sim 10^{10} M_{\odot}$, and very long cooling times. There are currently only four such coronae detected.

Tidal Disruption of Stars by SMBHs: Tidal disruption events (TDEs) were first discovered as transient X-ray sources in the nuclei of galaxies, but they have since been appearing in all-sky surveys in the ultraviolet and optical. The nearest TDE to date, ASASSN-14li, was discovered on 2014 November 22 at magnitude $V=16.5$ in the galaxy VII Zw 211 at $z=0.0206$. A bright X-ray counterpart was observed with the *XMM* RGS starting 3 weeks later ([Miller, J. M., et al. 2015; Fig. 9](#)), and showed a 50 eV blackbody spectrum with an area consistent with the innermost stable circular orbit around a $\sim 2 \times 10^6 M_{\odot}$ black hole, and a luminosity around the Eddington limit. In a major surprise, blue-shifted, high ionization absorption lines were seen that had been predicted from the super-Eddington phase of the newly formed accretion disk. Since the outflow velocities are only a few hundred km s^{-1} , much less than the escape velocity from the absorption radius of $\sim 10^4 GM/c^2$, it is also possible that the absorber is a filament of disrupted stellar material near the apocenter of an elliptical orbit. Together with monitoring by the *Swift* and UV/Optical Telescope, these observations have

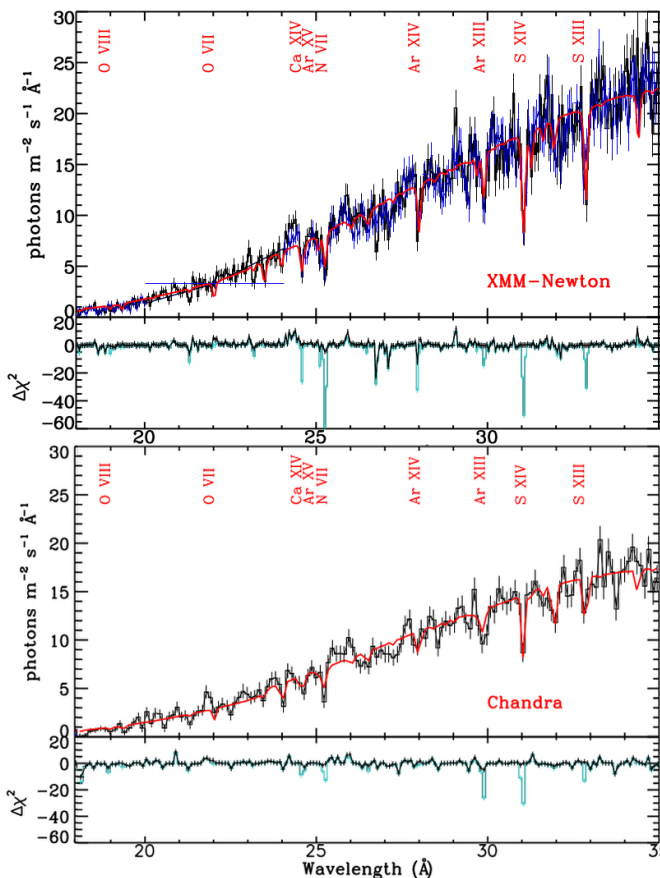


Figure 9. Grating spectra from XMM and Chandra of the tidal disruption event ASASSN-14li (Miller, J. M., et al. 2015). The best-fitted photoionized absorber model is in red, and the residuals are shown below both before (cyan) and after (black) modeling the absorbing gas (Miller, J. M., et al. 2015).

confirmed detailed theoretical predictions for the structure and evolution of TDEs.

Recently, a likely stellar tidal disruption event was found retrospectively in the 3XMM-DR5 SSSC (Lin et al. 2015). The host galaxy SDSS J152130.72+074916.5 ($z=0.17901$) was observed as part of an XMM observation on 2000 August 23. The average X-ray luminosity was $\sim 5 \times 10^{43}$ erg s^{-1} (0.24–11.8 keV, unabsorbed). Short-term variability in both the flux and spectrum was seen during the XMM observation. The source was not detected by Chandra on 2000 April 3, by Swift on 2005 September 10, or in a second XMM observation on 2014 January 19, implying variability by a factor of $\gtrsim 300$. The optical spectrum of the nucleus of the host galaxy showed no signs of activity roughly 11 years after the XMM detection. The XMM spectrum is well-fitted by a cool thermal disk with an disk temperature of 0.17 keV and a fast-moving warm absorber. Lin et al. (2015) attribute the fast-moving warm absorber to the super-Eddington outflow associated with the accretion event, and the short-

Future External Galaxy Research

It is likely that the XMM will continue to detect (particularly through studies utilizing the SSC, SSSC, OM SUSS, and OMCat) additional tidal disruption events. In addition, in AO-14/15, XMM accepted 3 LP/VLP proposals in the field of galaxy research, including: a detailed study of the diffuse emission in the spiral galaxy M31 was well as the point source population; XMM observations of the edge-on spiral NGC 891 which will determine how much of the halo gas is due to infall of intergalactic gas as opposed to material expelled from the disk, and derive the composition of the halo out to 8 kpc from the disk; and the Draco dwarf spheroidal, which is strongly dark matter dominated and contains very little hot gas, will be observed to detect the X-ray line at 3.5 keV which is possibly the signal of dark matter decay.

term variability to a disk instability that changed the inner disk radius but not the accretion rate.

1.4.4 Diffuse X-rays from the Milky Way (MW)

The Galactic Halo: Galactic halos are thought to contain a significant fraction of the “missing” baryons and may, in some models, be responsible for quenching star-formation. The Galactic halo is the only such halo that we can study in detail, either through emission, through absorption, or through its effect on cool gas clouds that may be embedded in it. Such studies of faint objects require a large grasp and often a large FOV, both of which are provided by XMM. It is somewhat problematic that we observe the halo only through foreground absorption and emission. Shadowing studies (e.g., Henley & Shelton 2015; Henley et al. 2015a) use the foreground absorbing clouds to determine the relative strengths of the foreground and halo emission, and can be used to determine the spectrum of the halo. In the presence of a time-variable foreground, solar wind charge exchange (SWCX), this method can produce inaccurate results, and certainly contributes to the large scatter in the measured halo properties.

The shadowing studies suggest that the contribution of the local emission in O VIII is negligible, and that of O VII is small and calculable. As a result, Henley & Shelton (2013) and a series of earlier papers used the XMM archive to extract and fit the diffuse spectrum from every mostly-empty line of sight through the halo. They removed the foreground emission in a simple and consistent way, in order to isolate the halo emission. In that work, they had unsuccessfully attempted to determine the flattening of the Galactic halo from

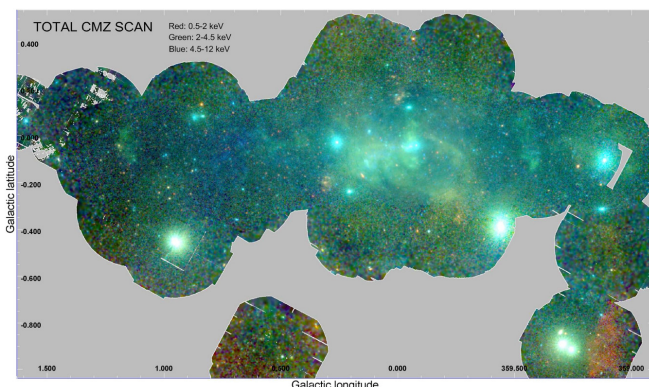


Figure 10. A false-color mosaic image of all XMM observations within 1° of Sgr A*. This represents the deepest X-ray view of the central MW with an exposure higher than 0.2 Ms along the Galactic disc and 1.5 Ms in the center. X-ray emission from X-ray binaries, star clusters, SNRs, bubbles and superbubbles, H II regions, PWNs, non-thermal filaments, nearby X-ray active stars, the SMBH Sgr A* and many other features are visible (Ponti et al. 2015).

the distribution of O VII lines strengths. Miller & Bregman (2015) have also used the Henley & Shelton database. Using different filtering to exclude poorer spectral fits and an improved treatment of the line strengths, they fitted the remaining O VIII data to a β -model to determine the mass of the Galactic halo. They find that the hot Galactic halo can account for $<50\%$ of the missing baryons. The O VII lines are more problematic because they contain emission from the Local Hot Bubble. Henley et al. (2015b) have compared the derived mean halo temperature and surface brightness to a pure supernova driven galactic fountain, and find that the fountain model is only slightly too cool, but roughly two orders of magnitude too faint. Together with more sophisticated modeling and the improved understanding of the SWCX, the Henley & Shelton database (and future updates) will continue to provide significant constraints on halo models.

Due to the tenuous nature of the Galactic halo, absorption line studies with the RGS require bright extragalactic targets, long (several 100 ks) exposures, and are generally limited to the O VII line. However, given the interest in AGNs, such observations have been slowly accumulating in the archive. Fang et al. (2015) studied the existing 43 AGN halo lines-of-sight and detected O VII absorption in 21. In some of these, it was even possible to fit the Doppler widths of the lines. The measured column densities are rather sharply peaked with a tail to larger values. There is no significant correlation of equivalent width (EW) with location. As RGS AGN studies acquire deeper observations on

existing and new targets, our understanding the distribution and dynamics of the Galactic halo will also improve.

The Galactic Center: The Galactic center is a rich astrophysical laboratory. Indeed, it sometimes appears to be too rich, with an abundance of different overlapping X-ray structures interleaved with multiple absorbing components, and perhaps modulated by magnetic fields that are only partially traced by the radio observations. However, after two dedicated surveys, an extended monitoring campaign for Sgr A*, and many observations of individual interesting objects, a new mosaic of the Galactic center by Ponti et al. (2015) unfolds the natures and relations of the various structures (Fig. 10). Heard & Warwick (2013) concentrated on the central 100 pc, showing that the emission in the bipolar lobes of Sgr A* is thermal and possibly powered by the central stellar cluster. Conversely, if they are powered by the central BH, they are consistent with the expected rate of stellar disruptions. Ponti et al. (2015) take a broader view of the region, estimating the star-formation rate from a more complete catalogue of SNRs, and reconsidering the energetics of the Sgr A* lobes. Even with this study, the Sgr A* lobes extend beyond the FOV, and a large project approved in AO-14 will extend this mosaic to the north and may potentially connect the lobes to the *Fermi* bubbles.

Light Echoes: Light echoes are a useful tool for exploring the distribution of dust in the MW, as demonstrated by Tiengo & Mereghetti (2006) and more recently by Heinz et al. (2015). Heinz et al. found several light echoes due to Galactic dust around the bright Galactic X-ray binary Circinus X-1, which underwent a strong X-ray flare in late 2013, and used them to determine its distance. The X-ray light echoes were imaged in February 2014 (shown in Fig. 18 below). Any bright X-ray flare, such as a γ -ray burst (GRB), can be used for such a study. The long-standing ToO triggers for such event suggest that exploration of the distribution of dust in the MW will continue over the next several years.

X-raying the Cool ISM: Absorption line spectroscopy of bright targets with the RGS measures abundances and ionization fractions that are in good agreement with optical determinations (Pinto et al. 2013) and reproduce the expected abundance gradient. Further, the absorption edges constrain the composition of dust (Valencic & Smith 2013), as well as provide a measure of the depletion. Measuring dust scattering halos in the X-ray places unique constraints on the size and porosity of dust; (Valencic & Smith 2015) have shown that there is no significant population of dust grains

Future Milky Way (MW) Diffuse Emission Research

Shadowing studies of the Galactic gaseous halo and better methods to correct for foreground SWCX will provide more information on the halo and decide what fraction of the MW baryons reside in it. Updates to the Henley & Shelton database (Henley et al. 2015b) will be particularly useful for this. Light echoes from GRBs, Galactic XRB flares, and other such sources will allow the distribution of dust in the MW to be determined. RGS spectra of bright AGNs will also give information on absorption by MW ISM along new lines of sight. The complex structure of diffuse emission in the Galactic Center will continue to be studied. In addition, in AO14/15, XMM accepted 2 LP/VLP proposals in the field of MW diffuse emission: XMM observations which will study the origin of the recently discovered warm plasma rising from the Galactic plane at the locations of the “Radio Arc” and the Sgr C thread in the Galactic plane; and a study of the origin of the diffuse X-ray emission along the Galactic ridge.

with radii $>0.5 \mu\text{m}$, and found no need for highly porous dust.

The correlation between the X-ray absorbing column towards pulsars and the radio-derived dispersion measure towards the same pulsars sets the mean ionization fraction of the local ISM to $\sim 10\%$ (He et al. 2013), confirming previous analyses using other measures of the intervening column density. In a slightly different environment, comparison of the absorbing column densities towards young stars determined through X-ray spectroscopy have been compared to column densities determined through Ly α and A $_v$ measurements to probe the circumstellar environments (McJunkin et al. 2014).

1.4.5 Exoplanets, Star Formation, and Stellar Evolution

Star-Planet Interactions: The discovery of hot Jupiter systems around young and old G-, K- and M-type host stars has stimulated the study of the effect of X-ray irradiation on planetary atmospheres, star-planet interactions, the possible spin-up of host stars by hot Jupiters, and the resulting increase in magnetic activity. The importance of X-rays (as ionizing radiation, and as a reliable proxy for magnetic activity) has prompted renewed interest in detailed studies of magnetic activity cycles across the H-R diagram.

Miller, B. P., et al. (2015) used a sample of over 200 main-sequence hosts with close-in giant planets to look for evidence of planet-induced

coronal and chromospheric activity. They found a significant increase in X-ray luminosity with $M_p a^{-2}$, where M_p is the planet mass and a is the planet semi-major axis. However, the increase in the sample is driven primarily by a handful of extreme hot Jupiter systems with $M_p a^{-2} > 450 M_J AU^{-2}$. Poppenhaeger & Wolk (2014) found that two systems with strong tidal interactions showed significantly higher coronal X-ray activity levels, while the three systems with the lowest tidal interactions did not.

In a detailed RGS study of the nearby, active, eclipsing hot-Jupiter system HD 189733 A, Pillitteri et al. (2014a) found enhanced flare activity during eclipse. Because the star-planet separation is only $8 R_\star$, they suggest the flares may be triggered by the planet as it passes through the magnetic loops of the host star. A light curve analysis suggests a local magnetic field strength of 40–100 G.

Star Formation: XMM studies continue to probe the origin of the X-ray emission from classical T Tauri stars, and the impact of X-rays on protoplanetary discs. Robrade et al. (2014) used a deep XMM observation of the M0 accreting T-Tauri star DN Tauri to show that much of the X-ray activity is coronal, but that the coolest, densest plasma originates in time-variable accretion shocks. Ercolano et al. (2014) confirm the correlation between accretion rate and stellar mass, and show that the M-M $_\star$ relation in pre-main-sequence stars is a direct result of viscous accretion and X-ray photoevaporation.

Magnetic Activity and Coronal Activity Cycles: The importance of star-exoplanet interactions has provided additional impetus for understanding magnetic activity and coronal activity cycles on late-type stars. Ayres (2014) reports on the long-term monitoring of α Centauri A and B with Chandra and XMM, revealing an 8.1 ± 0.2 yr activity cycle in the old K1 dwarf α Cen B. Meanwhile the G2 V star α Cen A appears to be emerging from a ten-year low state. Though A's low state could be like a Maunder minimum, Ayres suggests it is an overlong cycle, implying a cycle period of 19.2 ± 0.7 yr. In contrast to the older α Centauri system, the active, 600-Myr old, solar-like star ι Horologii has the shortest known chromospheric activity cycle: 1.6 yr. Sanz-Forcada et al. (2013) report the first X-ray activity cycle from an active star, confirming its primary cycle period, and suggest a second, longer cycle period.

Using archival ROSAT, XMM, and GALEX data, Stelzer et al. (2013) established a broadband ultraviolet-X-ray flux relation for a volume limited sample of M dwarfs (within 10 pc). The spread in UV/X-ray activity and rotation is widest at spectral

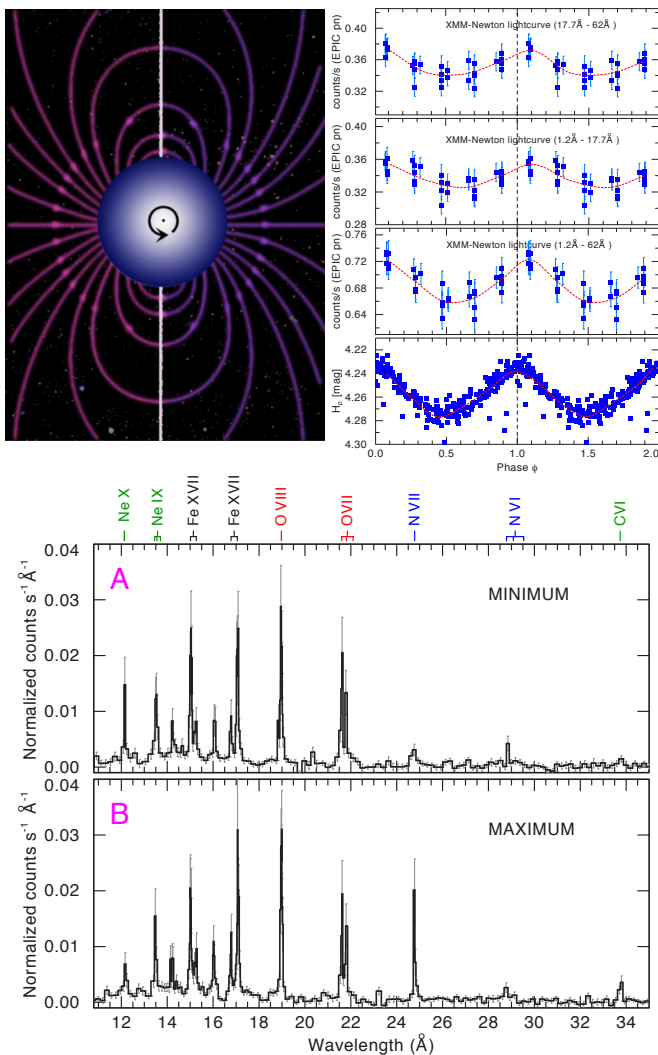


Figure 11. A new type of X-ray pulsar discovered with XMM (Oskinova et al. 2014). This is the first X-ray pulsar not associated with a degenerate star. Upper left panel: Rotational and magnetic geometry of the magnetic β Cep pulsator ξ^1 CMa. The curved lines illustrate the dipole magnetic field geometry. The star is viewed nearly along the rotational axis. The star is a magnetic oblique rotator: its magnetic and rotational axes are inclined to each other by 79° . Hence the magnetic equator (white stripe) is always seen nearly edge-on. Thus, the X-ray variations are not caused by rotation. Upper right panel: XMM EPIC pn X-ray count rate in soft, medium, and hard bands (three upper panels) and Hipparcos optical magnitude (lowest panel) light curves of ξ^1 CMa, phased with the stellar pulsation period of 0.209577 d. Lower panel: Combined XMM RGS1+RGS2 spectra of ξ^1 CMa in phases close to the pulsation minimum (upper panel, $\phi=0.5\pm 0.17$) and pulsation maximum (lower panel, $\phi=0.0\pm 0.15$), respectively. Strong emission lines are identified. The plasma is somewhat hotter at X-ray maximum. The nitrogen abundance, inferred from N VII Ly α , appears to double near X-ray maximum.

type M4, and activity decreases by nearly three orders of magnitude from the age of the TW HyA association (10 Myr) to a few Gyr in the broader sample. As activity increases, flux shifts from the chromosphere (near UV [NUV], and H α emission) to the corona and transition region (X-ray and far UV [FUV] emission).

Massive Stars: The brightest stellar X-ray sources are the massive luminous blue variables (LBVs), Wolf-Rayet stars, and OB stars, whose X-ray emission is connected to their strong winds, producing relatively soft embedded wind shocks in single stars (Cohen et al. 2014), colliding wind shocks in massive binaries (Lomax et al. 2015; Parkin et al. 2014; Hamaguchi et al. 2014), and modulated X-rays in magnetic wind shocks in the massive stars with magnetospheres (Nazé et al. 2014a, 2015; Pillitteri et al. 2014b). Nazé et al. (2014b) performed a systematic study of all known magnetic massive stars with X-ray data. They find that the X-ray luminosity is strongly correlated to stellar mass-loss rate, consistent with the latest magneto-hydrodynamic (MHD) models of magnetospheric X-ray emission.

On one of these magnetic stars, the β Cep pulsator ξ^1 CMa, Oskinova et al. (2014) report X-ray pulsations with the same period as the fundamental stellar oscillation. These are the first X-ray pulsations detected from a non-degenerate star (Fig. 11). The upper left panel shows the rotational and magnetic geometry of this star. We view the star nearly along the rotation axis, and the magnetic axis is almost orthogonal (the projection of the magnetic equator is the white line in the figure). Thus, the pulsation is not due to rotation. The upper right panel shows that the X-ray pulsations occur with the same period and nearly in phase with the optical pulsations. The lower panel shows that the X-ray pulsations are accompanied by significant changes in the X-ray spectra, and particularly the strength of the N VII Ly α line.

Stellar X-ray Bubbles: Soft, diffuse X-ray emission is now being routinely detected from the hot plasma within planetary nebulae (PNe) (Guerrero et al. 2015). In Fig. 12 we show the “born-again” PN A78, an X-ray twin of A30. Both PNe show a central point source, and diffuse, soft X-rays associated with shocks between the H-poor ejecta and the current, fast stellar wind (Toalá et al. 2015a).

Recently, diffuse X-rays have been found within nebulae associated with Wolf-Rayet stars: NGC 2359 and WR 7 (Toalá et al. 2015b; Zhekov 2014), NGC 6888 and WR 136 (Toalá et al. 2014, 2015c) and S 308 and HD 50896 (Toalá et al. 2012).

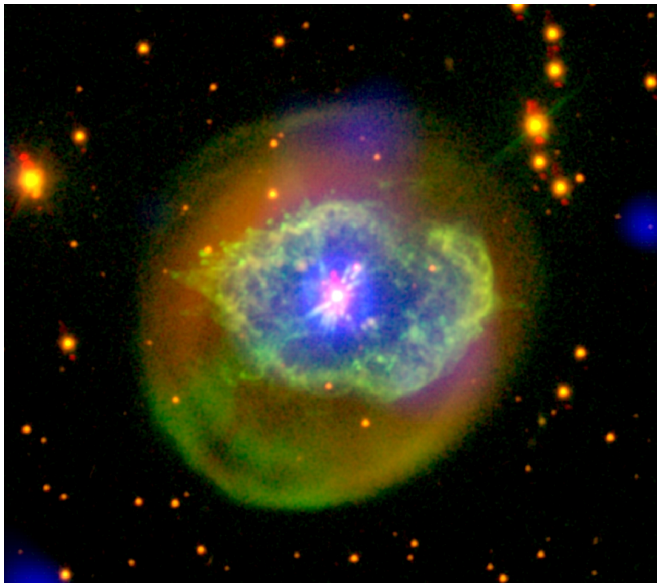


Figure 12. Comparison of ground-based, narrow-band optical and XMM images of the “born-again” planetary nebula A78 (Toalá et al. 2015a), showing the large-scale spatial distribution of O III (red), H_{α} (green) and 0.19–0.60 keV X-ray emission (blue).

Figure 13 is a composite image of NGC 6888 showing X-ray emission in blue, O III emission in green, and H_{α} emission in red. The EPIC image shows three lobes of emission and temperature/nitrogen abundance gradients within the nebula, suggesting differential mixing. They find electron densities of $\sim 0.4 \text{ cm}^{-3}$, plasma temperatures of a few MK, and total plasma mass of $1\text{--}2M_{\odot}$.

Star Clusters: Star-forming regions, OB associations, and open star clusters are ideal targets for the EPIC MOS and PN cameras on XMM because they contain hundreds to thousands of coeval young stars spanning the entire initial mass function. With ground-based optical and near-infrared observations, XMM studies continue to identify new clusters and cluster members (e.g., Mooley & Singh 2015; Ramage Evans et al. 2014).

1.4.6 Supernovae and Gamma-Ray Bursts

XMM studies of GRBs and SNe made some groundbreaking discoveries over the past few years. XMM has been instrumental in providing detailed X-ray data for GRB afterglows to constrain their origins. Recently these data were essential to uncovering the source of intrinsic X-ray absorption in these events, which turns out to be mostly the He in their parent star-forming regions (Watson et al. 2013), with some possible contribution from the intergalactic medium (IGM) as suggested by the correlation of absorption with redshift (Starling et al. 2013; Campana et al. 2014).

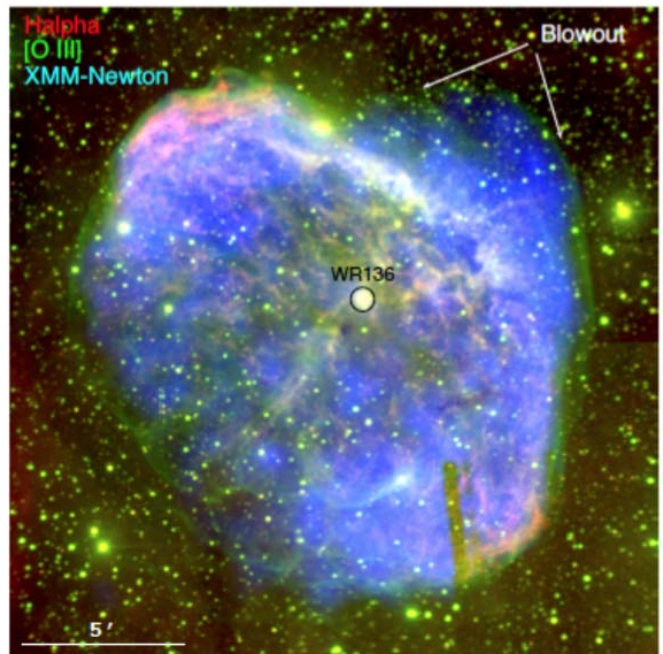


Figure 13. Composite image of the NGC 6888 bubble around Wolf-Rayet star WR 136 (Toalá et al. 2015c). X-ray emission is shown in blue, O III emission in green, and H_{α} emission in red. EPIC imaging spectroscopy suggests temperature/nitrogen abundance variations across the nebula.

Future Stellar Research

XMM will continue to study the effects of X-ray emission from protostars on star formation and protoplanetary discs. New stellar clusters and new members of clusters will be identified. Hopefully, new X-ray pulsators, similar to the magnetic massive star $\xi^1 \text{ Cma}$, will be detected, and there is an AO-14 LP proposal to do this. In AO-14/15, XMM accepted 4 LP/VLP proposals in the field of stars and exoplanets, including: an XMM/Kepler program to provide X-ray flare energies and statistics for flares on stars covering a range of spectral types in the Pleiades and Praesepe in order to understand the flare energy release on stars through time, the impact of stellar flares and activity on exoplanets, and the fundamental efficiency of magnetic dynamos in dissipating energy; a snapshot survey of K and M dwarf stars in the Hyades cluster to determine the relationship between stellar magnetic activity and rotation, and the origin of the magnetic saturation threshold where, for unknown reasons, activity no longer varies with rotation period; and a project to determine the X-ray spectra of a representative sample of active star binaries (ASBs), in part to determine if they dominate the unresolved emission in the Galactic ridge.

Two particularly interesting bursts over the past 2 years were observed by *XMM*. One was the short GRB 130603B, where *XMM* found a peculiar X-ray excess that may indicate the formation of a magnetar (Fong et al. 2014). Another was the ultralong GRB 130925A, where *XMM* uncovered a second, hard, X-ray emission component in the late stages of the burst, possibly indicating a very low metallicity progenitor (Piro et al. 2014). Finally, long-term *XMM* and optical follow-ups of a low luminosity GRB found a shock break-out signature, supporting a failed-jet model for unifying low and high luminosity GRBs (Schulze et al. 2014).

Recent *XMM* follow-ups of SNe have also resulted in new discoveries. Margutti et al. (2014) and Ofek et al. (2013) shed new light on SN2009ip as a very bright eruption associated with mass loss episodes of a massive star in the late stages of evolution. The *XMM* observations of this object reveal mass-loss rates of up to $10^{-2} M_{\odot} \text{ yr}^{-1}$ leading up to the latest eruption, putting new, challenging requirements on models of massive stellar evolution. Ofek et al. (2014) made one of the first direct measurements of a SNe shock velocity just 2 years after maximum light. The *XMM* data constrain the shock velocity to 2000–5000 km s⁻¹ depending on the equilibrium state of the electrons and ions in the shock.

1.4.7 Supernova Remnants (SNRs)

With its large field of view and soft sensitivity, *XMM* is particularly well-suited to the study of SNRs. For example, Seitzzahl et al. (2015) recently found that with these attributes *XMM* is the best instrument to distinguish between competing progenitor models for SN Ia explosions in events at distances $\leq 1\text{--}2$ Mpc. Over the past few years, SNRs have been at the heart of several fundamental science investigations, from dark matter physics to massive stellar evolution.

Galactic SNRs: There were several breakthrough studies of individual Galactic SNRs recently from *XMM* observations. Gelfand et al. (2013) employed *XMM* observations of Kes 17 in a multi-wavelength study showing that it produces cosmic rays very efficiently, likely due to its location within a molecular cloud. Broersen et al. (2014) were able to put tight constraints on the progenitor of SN 185 A.D. based on chemistry and morphology from *XMM* data. They were effectively able to model the entire history of the SNR as a Type Ia from a single-degenerate system exploding in a wind-blown cavity. Sasaki et al. (2014) and Kumar et al. (2014) find strong evidence for massive progenitors for SNR W51C and SNR Kes 73, respectively. Deep observations

of SN1006 have now been completed, including grating spectroscopy, allowing a direct thermal broadening temperature measurement of the shocked oxygen of 275 keV (Broersen et al. 2013), with an electron temperature of only 1.4 keV, quantifying the non-equilibrium state of material in SNR shocks. Chiotellis et al. (2013) successfully modeled Tycho’s SNR with a Type Ia inside of a wind bubble, which provides new clues for single and double-degenerate Type Ia progenitor theory.

Extragalactic SNRs: *XMM* has also been at the forefront of extragalactic SNR studies. For example, over the past few years, *XMM* has provided many exciting discoveries of and constraints on SNRs in the Magellanic Clouds. Maggi et al. (2014) discovered 4 new LMC SNRs with deep *XMM* observations, at least 2 of which appear to be from Type Ia events. Bozzetto et al. (2014) were able to definitively identify a 70 pc diameter newly-discovered LMC SNR as a Type Ia, with separate X-ray bright, optically-bright, and radio-loud features (see Fig. 14), providing new constraints on the multiwavelength evolution of Type Ia SNRs.

XMM’s large FOV has enabled comprehensive X-ray studies of superbubbles, resulting in new discoveries about their energetics in the past 2 years. Reyes-Iturbide et al. (2014) performed a detailed thermal study of superbubbles in LMC, finding significant energy above that expected from stellar winds and radiation, constraining the amount of energy from SNe. These are not simply wind-blown superbubbles. Zhang et al. (2014a)

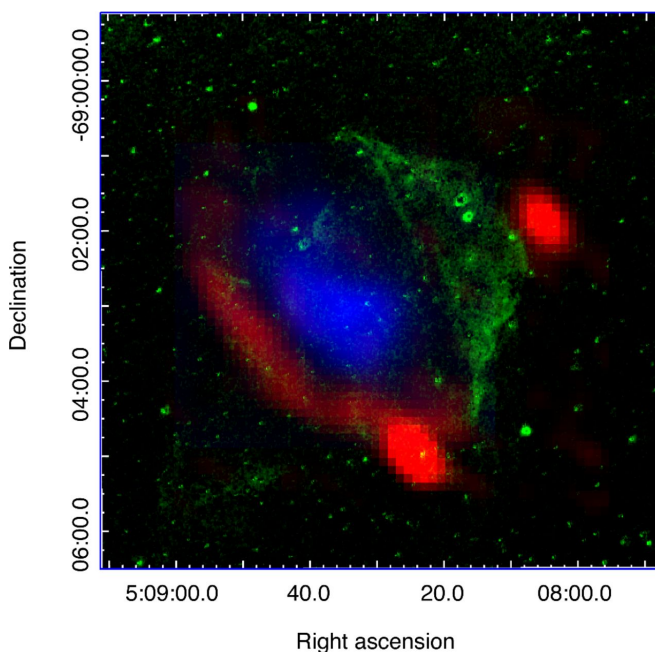


Figure 14. Radio (5500 MHz, red), Optical ($H\alpha$, green) and X-ray (0.7–1.1 keV, blue) emission of LMC SNR J0508-6902. (Bozzetto et al. (2014)

Future SNRs Studies

Surveys of the Galactic plane by HESS continue to discover extended TeV sources that appear to be new shell-type SNRs. Follow-up observations by *XMM* will evaluate these classifications and search for associated thermal plasma and synchrotron emission from accelerated electrons. They will also test leptonic and hadronic models for the TeV emission.

found a similar result for two large (>100 pc) nebulae in the LMC (N70 and N185), where both were found to have been energized by interior SNRs. [De Horta et al. \(2014\)](#) also find N70 to have likely been partially energized by past SNe. The evidence appears to be building against simple windblown super-bubbles.

1.4.8 Neutron Stars (NSs)

NSs are laboratories for the study of the equation of state of matter at densities higher than nuclear, while their populations are a tracer of massive star formation and a window into the physics of supernova explosions. The high-throughput spectroscopy and timing simultaneously available with *XMM* EPIC are needed to determine the physical properties of the majority of isolated pulsars that are radiatively inefficient at all wavelengths, and are often only detectable in X-rays. X-ray measured spin-down rates determine the pulsars' ages, dipole magnetic field strengths, and spin-down luminosity.

Central Compact Objects (CCOs): Particularly useful for measuring NS temperatures and radii are the ~ 10 CCOs in shell-type SNRs. CCOs have purely thermal X-ray spectra, uncontaminated by non-thermal emission, and many of them have relatively good distance estimates, which is important for measuring their radii. Their apparent blackbody radii are only a few kilometers, significantly smaller than the 10–15 km canonical NS. In some cases, this discrepancy can be resolved by fitting the spectra with hydrogen atmosphere models which, because of decreasing free-free opacity with increasing energy, require lower effective temperatures and larger radii than a blackbody fit. However, two-temperature thermal models are required in most cases, even for CCOs that show no rotational modulation, such as the prototype of the class, the CCO in Cas A. For the latter, a solution of this apparent paradox was proposed in the form of a uniform temperature carbon atmosphere model, which yields both a good fit to the spectrum and a reasonable radius of 10–14 km ([Ho & Heinke 2009](#)).

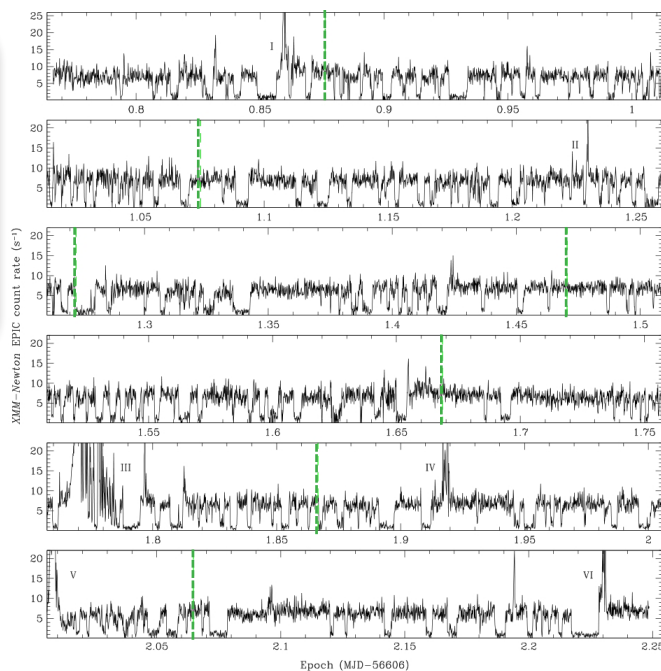


Figure 15. A continuous 1.5 day *XMM* EPIC light curve of PSR J1023+0038 in the 0.3–10 keV band, acquired during 2014 June 10–11. The vertical dotted lines mark the times of superior conjunction of the pulsar in the 4.75 hr binary. The Roman numerals mark six prominent flares ([Bogdanov et al. 2015](#)).

A minority of CCOs have pulsations; the largest amplitude is 64% for the CCO in Kes 79, which cannot be accommodated by any uniform surface temperature model. While its surface dipole field measured from spin-down is only $B_s = 3.1 \times 10^{10}$ G, it is difficult to get a nonuniform surface temperature without invoking much stronger internal magnetic fields. [Bogdanov \(2014\)](#) modeled the *XMM* pulse profiles and spectra of the Kes 79 CCO to show that a strong ($\sim 10^{14}$ G) internal magnetic field is needed to channel heat to a small region on the surface, thus lending support to the theory that CCOs have normal magnetic fields that were initially buried by supernova fall-back debris. These fields can diffuse back out on a time scale of 10^4 – 10^5 yr, enabling the CCOs to merge with the ordinary radio pulsar population. This effect would be the physical basis of the CCO class, and such an evolution would explain why CCO descendants are apparently missing.

Magnetars: *XMM* continues to be the source of most of the spectra of Anomalous X-ray Pulsars (AXPs) and Soft Gamma-Repeaters (SGRs) that are being used to understand the emission mechanisms and B-field configurations of magnetars. A leading model, the twisted magnetosphere ([Beloborodov 2009](#)), produces both surface thermal hot spots at the footpoints of the field-line bundles, and

resonant cyclotron scattering of the thermal X-rays by strong currents in the magnetic loops. [Weng et al. \(2015\)](#) developed a 3D Monte Carlo model that applies the features of the twisted magnetosphere model to the *XMM* spectra of 13 magnetars to fit for four parameters: surface temperature, surface magnetic field strength, magnetospheric twist angle, and electron velocity. They concluded that the twist angles are large, >1 radian, and that twisting and untwisting are observed in the outburst of the AXP 1E 2259+586.

Millisecond Pulsars: With its high throughput and fast timing capability, *XMM* is playing a key observational role in the new field of transitional MSPs. These rapidly spinning NSs are theorized to originate in LMXBs where they are spun up (recycled) to millisecond periods by accretion, and emerge as rotation-powered, radio MSPs when the accretion stops. Beginning in 2013, switching back and forth between rotation-powered and accretion-powered states was recognized in three MSPs binaries, supplying the missing link between the radio MSPs and their LMXB progenitors. When accreting material penetrates within the light cylinder of the radio pulsar and falls onto the polar caps, it quenches the radio pulsation mechanism and replaces it with X-ray pulsations.

The archetype of the transitional MSPs is the 1.69 ms PSR J1023+0038, which has been in an accreting mode since June 2013. Long *XMM* observations of PSR J1023+0038 were obtained in 2013 November and 2014 June ([Bogdanov et al. 2015](#); **Fig. 15**). The resulting X-ray light curve re-

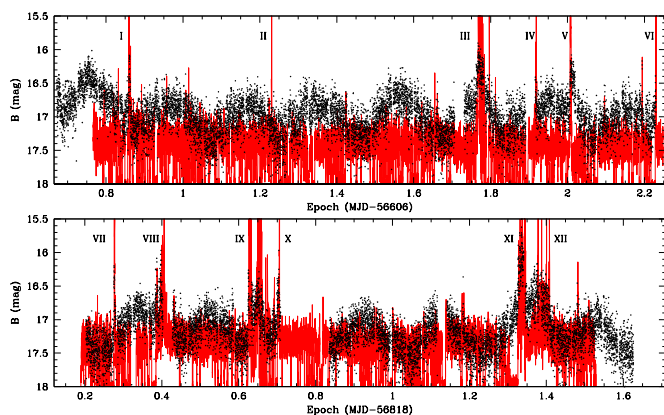


Figure 16. XMM OM fast mode light curve of PSR J1023+0038 in the B filter from 2013 November (top) and 2014 June (bottom). Each black point corresponds to a 10 s exposure. The error bars are omitted for the sake of clarity but are typically ± 0.2 mag. The 0.3–10 keV X-ray light curve (red) is plotted to show the relative alignment between the X-ray and optical flares. Gaps in the optical data are due to interruptions in exposure ([Bogdanov et al. 2015](#)).

Future Neutron Star Research

The *XMM* EPIC pn is the most capable current instrument for timing of fast, faint pulsars, as well as the most sensitive for the detection of X-ray pulsars in general. It will be used to study the recycled pulsars that continue to be found in large numbers by radio follow-up of Fermi sources, and to identify more members of the new class of transitional MSPs by their distinctive X-ray light curves. The faint, quiescent counterparts of new transient magnetars that appear on a yearly basis will be studied. Extended monitoring periods will be necessary in some cases to measure their dipole magnetic fields via spin-down, and to track their behavior into quiescence. *XMM* spectra are at the forefront of efforts to establish a unified theoretical understanding of magneto-thermal evolution of CCOs, magnetars, and other young NSs, e.g., [Vigano et al. \(2013\)](#). In addition, there is an *XMM* AO-14 LP to study the “Magnificent Seven” isolated neutron star RX J1605.3+3249 as an evolutionary link between magnetars and normal young pulsars. The aim is to understand why magnetars rotate more slowly, are hotter, and have higher magnetic fields than other pulsars of similar age.

vealed the unique phenomenology of the transitional MSP in the accretion-disk dominated state: stochastic changes between two discrete X-ray flux levels, called “high” and “low,” manifest as rapid and frequent drops in X-ray flux by nearly an order of magnitude in 10 s. These flux “drop-outs” are aperiodic, have no preferred duration, and are thus of an entirely different origin from the orbital-phase-dependent dips that define the X-ray dipper variety of LMXBs. A plausible interpretation for this peculiar behavior is the emptying and refilling of the inner disk. While the X-ray luminosity in the high state is $\sim 3 \times 10^{33}$ erg s $^{-1}$, occasional flares reach up to 10^{34} erg s $^{-1}$. Identical behavior is seen in the *XMM* light curves of the other transitional MSPs XSSJ12270-4859 ([de Martino et al. 2013](#)) and IGR J18245-2452 ([Ferrigno et al. 2014](#)).

Simultaneous OM observations of PSR J1023+0038 (**Fig. 16**, [Bogdanov et al. 2015](#)) reveal the 4.75 hr orbit via heating of the companion, as well as rapid optical flaring that coincides with some of the X-ray flares. Some of these flares are very short, lasting less than 1 minute, with rise times that are unresolved at the 10 s cadence of the data, showing that they are a phenomenon of the accretion disk.

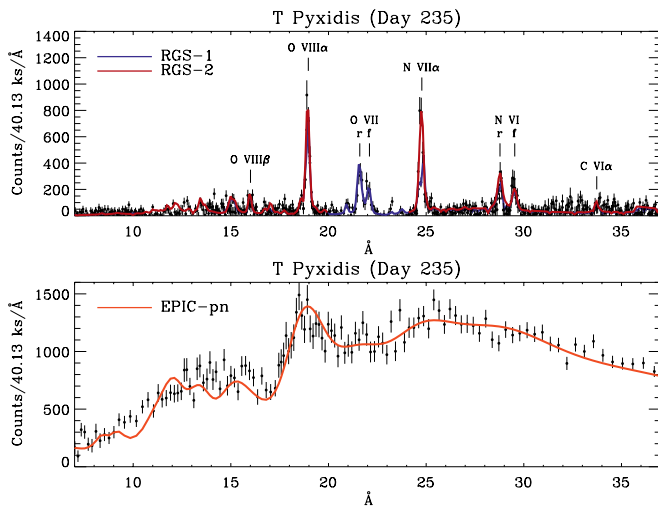


Figure 17. Binned XMM spectra of T Pyxidis 235 days after discovery. Top: RGS-1 and RGS-2 with model overlaid in blue and red, respectively. Bottom: concurrent EPIC-pn spectrum with model overplotted (Tofflemire et al. 2013).

Also in 2013, XSSJ12270-4859 was observed by XMM to have made the opposite transition, to an accretion-free, rotation-powered state (Bogdanov et al. 2014a; de Martino et al. 2015). In this state the light curve is completely different. While no X-ray pulsations are detected, the flux is smoothly modulated at the orbital period, and arises in the long-predicted intra-binary shock between the pulsar wind and the ablated face of the companion. The X-ray maximum at superior conjunction of the companion star places the shock very close to the companion star. Transitional MSPs are drawn from the larger population of nearly Roche-lobe-filling “redbacks,” which are related to the black-widow pulsars, the energetic MSPs that have nearly evaporated their companion stars. These and other eclipsing millisecond pulsars that were once rare are being found in large numbers by *Fermi*, and are being studied very effectively by XMM (e.g., Bogdanov et al. 2014b; Roberts et al. 2015; Romani 2015).

1.4.9 Cataclysmic Variables (CVs) and X-ray Binaries (XRBs)

CVs: T Pyxidis is a famous recurrent nova that had recorded outbursts in 1890, 1902, 1920, 1944, and 1966. Long overdue, the most recent outburst in 2011 was intensively studied at all wavelengths. X-ray grating observations were obtained by XMM 235 days after the outburst (Tofflemire et al. 2013; Fig. 17). The spectra are dominated by emission lines, with the He-like triplets (resonance, inter-combination, forbidden) of O VII and N VI providing temperature and density diagnostics. The lines

originate in dense clumps ($n_e \sim 10^{10} \text{ cm}^{-3}$) of plasma in collisional ionization equilibrium (CIE). This was used to argue that the emission may be due to internal shocks from the interaction of shells of different velocity within the ejecta. The lines have widths of $\sim 2400 \text{ km s}^{-1}$, with the centroid of the highest ionization lines blueshifted by a few hundred km s^{-1} , indicating partial absorption in the receding side of the flow.

The continuum X-ray spectrum of the super-soft source was visible at the time of the observations, and was fitted with a white dwarf model atmosphere of $T \sim 4.2 \times 10^5 \text{ K}$. This is much cooler than in other recurrent novae, implying a white dwarf in T Pyx of $\sim 1 M_\odot$, which is significantly below the Chandrasekhar mass. Since the ejected mass is estimated to be 10^{-5} – $10^{-4} M_\odot$, more mass is lost in the eruptions of recurrent novae than is accreted between outbursts, which would reduce the white dwarf mass over time.

XRBs in the Milky Way: Circinus X-1 is a highly variable X-ray binary that has often been characterized as erratic. It has been difficult to classify in terms of canonical X-ray binary schemes, combining properties of young and old X-ray systems. The presence of type I X-ray bursts identifies the compact object as a NS with a low magnetic field, suggesting a classification as an old, LMXB with an evolved companion star. This interpretation is in tension with the observed orbital evolution time

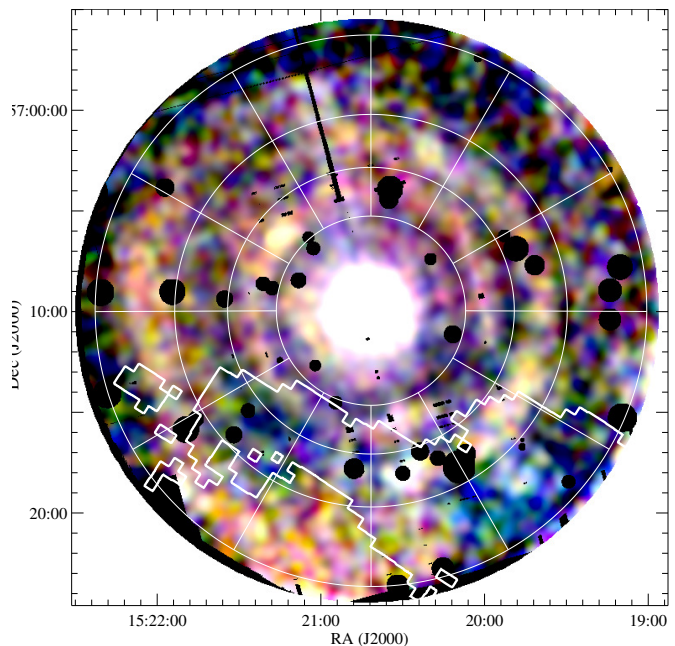


Figure 18. XMM EPIC image of the dust echoes from Circinus X-1 on 2014 February 17. The overplotted white line is a ^{12}CO contour in the velocity range -33.6 to -29.6 km s^{-1} (Heinz et al. 2015).

Future X-ray Binary Research

In AO-14/15, *XMM* accepted 2 LP/VLP proposals in the field of XRB research. First, iron K line Doppler tomography of the black hole binary H 1743-322 will be used to test the theory that its 4s QPO is driven by relativistic precession. There is evidence that the iron line centroid varies during the QPO. Second, a deep observation of the ULX in a globular cluster in the Virgo Cluster elliptical NGC 4472 will be used to understand the variability of the likely ultracompact black hole and to place important constraints on whether beaming can explain the high luminosities of ULXs.

of order 3000 yr, and the possible identification of an A-B supergiant companion, suggesting a much younger age. The conflict was resolved with the discovery of an arcminute scale supernova remnant in both X-ray and radio (Heinz et al. 2013), making Circinus X-1 the youngest known X-ray binary. Still, its distance and X-ray luminosity remained highly uncertain.

XMM and *Chandra* (Heinz et al. 2015) observations of a bright flare of Circinus X-1 serendipitously revealed one of the largest and brightest set of rings observed to date from an X-ray light echo (Fig. 18). The four well-defined rings with radii from 50 to 130 pc, growing in radius with time, are due to four intervening dust concentrations. The association of the rings with individual CO clouds having particular radial velocities, and the time delays of the scattered X-rays allowed a precise determination of a distance of 9.4–1.0 kpc to Circinus X-1. This implies that Circinus X-1 is frequently a super-Eddington source, and places a lower limit of $\Gamma > 22$ on the Lorentz factor of its radio jet, and an upper limit of 3° on the jet viewing angle from the line of sight.

ULXs in External Galaxies: The ongoing debate as to whether ULXs represent sub-Eddington accretion onto an intermediate-mass black hole (IMBH) or super-Eddington accretion onto a stellar mass black hole, or both, continues to evolve with the help of *XMM*. Coordinated *NuSTAR* and *XMM* observations of several ULXs gave near-simultaneous spectral coverage from 0.3–25 keV and showed that the high energy X-ray spectra of ULXs roll over above 10 keV (Bachetti et al. 2013; Walton et al. 2015a,b). Such spectra are inconsistent with the canonical low/hard accretion state in MW stellar-mass black hole binaries arguing for super-Eddington accretion onto a low-mass black hole.

1.4.10 Cosmology, Surveys, and Serendipitous Science

XMM deep observations of selected fields have enlarged and enhanced our understanding of the Universe in a wide variety of areas from results on star clusters, the Galactic plane, nearby galaxies, the evolution of clusters of galaxies, and AGN population properties and evolution. In addition to these focused surveys *XMM* has produced the following general purpose catalogs.

Serendipitous Source Catalog: The SSC⁶ includes all of the *XMM* public data (Rosen et al. 2015). With major improvements to the *XMM* data reduction algorithms, the catalog has enhanced source characterization, reduced spurious source detections, refined astrometric precision, provided greater net sensitivity for source detection, and allowed the extraction of spectra and time series for fainter sources with better S/N. With 50% more data compared to 2XMMi-DR3, the DR5 catalog has 565,962 X-ray detections comprising 396,910 unique X-ray sources, the largest X-ray source catalogue ever produced.

For the 133,000 brightest sources, spectra and light curves are provided. For all the sources information about the variability, and count rates in 7 X-ray energy bands, are provided. All the sources are cross-correlated with 228 catalogs to provide identifications. This catalog has been well used scientifically with recent results as diverse as the detection of a tidal disruption candidate at the SMBH in a distant galaxy (Lin et al. 2015) to adding new X-ray detections in nearby stellar clusters (Murphy et al. 2015). The 3XMM-DR5 catalog is a major resource for a nearly unlimited range of astrophysical research.

Slew Survey Source Catalog: The SSSC⁷ is the largest solid angle 2–8 keV survey ever performed (Fig. 19, Read et al. 2011). Currently it covers about 65% of the sky to a flux limit of 3×10^{-12} erg cm⁻² s⁻¹, 6× deeper than the best previous survey. It has over 6,000 sources in the 2–12 keV band and 2×10^4 sources in the 0.2–2 keV band with a sensitivity similar to the *ROSAT* Bright Source Catalog but better positions with a mean statistical position error of $\sim 4''$ for non-extended sources. Over 70% of the sources have been identified from catalogs and follow-up work. Until *eROSITA* finishes its survey, this is the most sensitive-all sky X-ray catalog.

Other catalogs based on these X-ray surveys: The availability of both of these catalogs

6 http://xmmssc.irap.omp.eu/Catalogue/3XMM-DR5/3XMM_DR5.html

7 http://xmm.esac.esa.int/external/xmm_products/slew_survey/xmms1d_ug.shtml

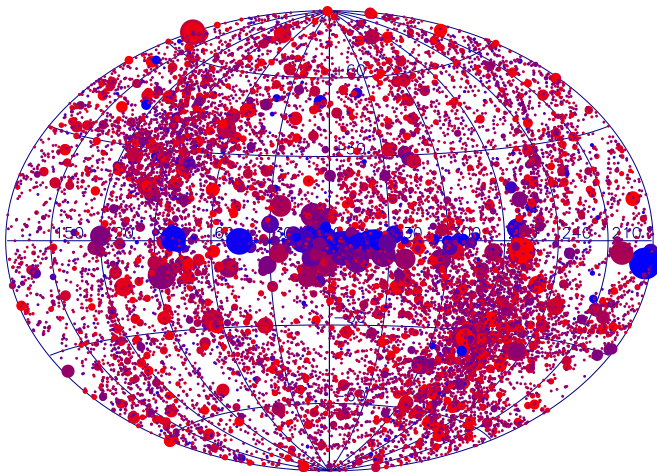


Figure 19. Sky-map of the SSSC data (Read et al. 2011), where area corresponds to the logarithm of the flux of the source and color corresponds to its X-ray hardness (blue-hard, light red-soft).

has engendered the Exploring the X-ray Transient and variable Sky (EXTrAS)⁸ project (De Luca & EXTrAS Collaboration 2015). It aims at fully exploring and making publicly available in an easy-to-use fashion the serendipitous content of the XMM Surveys in the temporal domain. The first science from this project (Belfiore et al. 2015) includes the detection of the first magnetar in M31.

The Astronomical Resource Cross-matching for High Energy Studies (ARCHES)⁹ aims at enriching the 3XMM catalog by building scientifically validated broad-band spectral energy distributions (SEDs) for a large fraction of the X-ray sources. The project is developing new tools for cross-correlations with extensive archival resources, producing well-characterized multiwavelength data in the form of SEDs for large sets of objects (e.g., Mateos et al. 2013; Gómez-Morán et al. 2016) and a catalogue of clusters of galaxies (e.g., Takey et al. 2014). ARCHES validates products and investigates their usability in the framework of a wide variety of science cases. All ARCHES products and tools will be made available to the general community. These enhanced resources will significantly broaden the effective exploitation of the XMM data by the scientific community.

OM Serendipitous UV Source Survey: An update of the OM SUSS 2.1 catalog¹⁰ of optical/UV sources detected serendipitously by the OM (Page et al. 2012) was released. It has 6,246,432 entries corresponding to 4,329,363 sources, of which 831,582 have multiple observations. For each entry, positional and photometric data (count rate, magnitude and flux) and quality flags for each

⁸ <http://www.extras-fp7.eu/>

⁹ <http://www.arches-fp7.eu>

¹⁰ http://www.mssl.ucl.ac.uk/www_astro/XMM-OM-SUSS

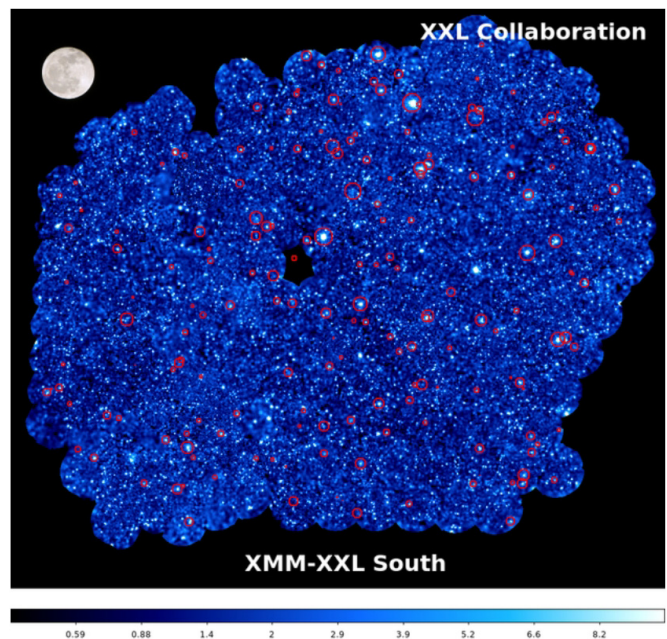


Figure 20. Mosaic of the southern region (about 25 deg²) of the XMM XXL survey, XMM's largest single project. All of the fields observed so far are shown. At the top left, the image of the Moon is given to scale; the Moon is about the same size as the XMM FOV. The red circles show clusters of galaxies. The data for this image, 698 exposures from 240 useful observations, were processed with the ESAS software developed by the GOF.

measurement are provided. As opposed to previous plans, a new incremental OM SUSS catalogue release is expected every year.

OMCat: The OMCat provides uniformly astronomically corrected data within the HEASARC format which allows easy access for archival studies of both point sources and extended objects. Unlike the OM SUSS, OMCat provides mosaicked, astronomically corrected images for each filter of each observation.

Focused XMM Surveys: The XXL is the largest XMM observing program to date, with almost 7 Ms in about 540 observations. The survey consists of 2 fields of 25 deg² each (XXL-North and

Future Survey Research

The SSC, SSSC, OMCat, and OM SUSS will continue to grow in size and importance over time, and continue to be a major resource in combination with other new multi-wavelength and multi-messenger observatories and surveys (e.g., LSST, eROSITA, LIGO, Ice-Cube). Value-added surveys such as EXTrAS and ARCHES will increase the impact of the XMM surveys by making associated data broadly available to scientists around the world.

XMM-Newton Senior Review Proposal

XLL-South) observed to a point source sensitivity of $\sim 5 \times 10^{-15}$ erg cm⁻² s⁻¹ (0.5–2 keV). **Figure 20** shows the South XXL field. Note that the analysis and mosaicking of these observations were done with the GOF-developed ESAS package (see the cover page for the uncorrected mosaic). In AO-15, XMM approved a “beyond COSMOS” survey of the XMM LSS field to a depth of 50 ks, which will find thousands of clusters of AGNs, and hundreds of clusters of galaxies. Recent results from this survey were released in Dec 2015 in a special issue of *Astronomy & Astrophysics* ([Pierre et al. 2016](#)).

XMM-Newton Senior Review Proposal

References

- Anderson, M. E., et al. 2015, MNRAS, 452, 3905
- Ayres, T. R. 2014, AJ, 147, 59
- Bachetti et al., M. 2013, ApJ, 778, 163
- Belfiore, A., et al. 2015, ATel #7181
- Beloborodov, A. M. 2009, ApJ, 703 1044
- Bogdán, _A., et al. 2013, ApJ, 772, 97
- Bogdán, _A., et al. 2015, ApJ, 804, 72
- Bogdanov, S. 2014, ApJ, 790, 94
- Bogdanov, S., et al. 2014a, ApJ, 789, 40
- Bogdanov, S., et al. 2014b, ApJ, 781, 6
- Bogdanov, S., et al. 2015, ApJ, 806, 148
- Boyarsky, A., et al. 2014, Phys. Rev. Lett., 113, 251301
- Boyarsky, A., et al. 2015, Phys. Rev. Lett., 115, 161301
- Bozzetto, L. M., et al. 2014, MNRAS, 439, 1110
- Broersen, S., et al. 2013, A&A, 552, A9
- Broersen, S., et al. 2014, MNRAS, 441, 3040
- Bulbul, E., et al. 2014, ApJ, 789, 13
- Campana, S., et al. 2014, MNRAS, 441, 3634
- Chiotellis, A., et al. 2013, MNRAS, 435, 1659
- Clavel, M., et al. 2014, MNRAS, 443, L129
- Cohen, D. H., et al. 2014, MNRAS, 444, 3729
- Dai, X., et al. 2012, ApJ, 755, 107
- De Horta, A. Y., et al. 2014, AJ, 147, 162
- De Luca, A., & EXTraS Collaboration. 2015, in Exploring the Hot and Energetic Universe: The first scientific conference dedicated to the *Athena* X-ray observatory, ed. M. Ehle, 55
- de Martino, D., et al. 2013, A&A, 550, A89
- de Martino, D., et al. 2015, MNRAS, 454, 2190
- Dennerl, K., et al. 2006, A&A, 451,709
- Ducci, L., et al. 2014, A&A, 566, A115
- Eckert, D., et al. 2014, A&A, 570, A119
- Ercolano, B., et al. F. 2014, MNRAS, 439, 256
- Fang, T., et al. 2015, ApJS, 217, 21
- Ferrigno, C., et al. 2014, A&A, 567, A77
- Fong, W., et al. 2014, ApJ, 780, 118
- Gelfand, J. D., et al. 2013, ApJ, 777, 148
- Gómez-Morán, A. N., et al. 2016, MNRAS, submitted
- Gonzalez, A. H., et al. 2013, ApJ, 778, 14
- Gu, L., et al. 2015, A&A, 584, L11
- Guennou L., et al. 2014, A&A, 561, A112
- Guerrero, M. A., et al. 2015, A&A, 574, A1
- Güver, T., et al. 2015, ApJ, 801, 48
- Hamaguchi, K., et al. 2014, ApJ, 784, 125
- He, C., Ng, C.-Y., & Kaspi, V., 2013, ApJ, 768, 64
- Heard, V., & Warwick, R. S. 2013, MNRAS, 434, 1339
- Heinz, S., et al. 2013, ApJ, 779, 171
- Heinz, S., et al. 2015, ApJ, 806, 265
- Henley, D. B., & Shelton, R. L. 2013, ApJ, 773, 92
- Henley, D. B., & Shelton, R. L. 2015, ApJ, 808, 22
- Henley, D. B., et al. 2015a, ApJ, 799, 117
- Henley, D. B., et al. 2015b, ApJ, 800, 102
- Ho, W. C. G., & Heinke, C. 2009, Nature, 462, 71
- Hodges-Kluck, E. J., & Bregman, J. N. 2013, ApJ, 762, 12
- Jeltema, T., & Profumo, S. 2015, MNRAS, 450, 2143
- Kaastra, J. S., et al. 2014, Science, 345, 64
- Kara, E., et al. 2014, MNRAS, 445, 56
- Kettula, K., et al. 2015, MNRAS, 451, 1460
- Koutroumpa, D., et al. 2012, A&A, 545, A153
- Kumar, H. S., et al. 2014, ApJ, 781, 41
- Kuntz, K. D., et al. 2008, PASP, 120, 740
- Kuntz, K. D., & Snowden, S. L. 2008, A&A, 478, 575
- Lanzuisi, G., et al. 2014, ApJ, 781, 105
- Lin, D., et al. 2015, ApJ, 811, 43
- Liu, Z., et al. 2015, MNRAS, 447, 517
- Lomax, J. R., et al. 2015, A&A, 573, A43
- Lovisari, L., et al. 2015, A&A, 573, A118
- Maggi, P., et al. 2014, A&A, 561, A76
- Malyshev, D., et al. 2014, Phys. Rev. D, 90, 103506
- Margutti, R., et al. 2014, ApJ, 780, 21
- Mateos, S., et al. 2013, MNRAS, 434, 941
- McJunkin, M., et al. 2014, ApJ, 780, 150
- Miller, B. P., et al. 2015, ApJ, 799, 163
- Miller, J. M., et al. 2015, Nature, 526, 542
- Miller, J. M., & Bregman, J. N. 2013, ApJ, 770, 118
- Miller, J. M., & Bregman, J. N. 2015, ApJ, 800, 14
- Mitsuishi, I., et al. 2013, PASJ, 65, 44
- Mooley, K. P., & Singh, K. P. 2015, MNRAS, 452, 3394
- Moretti, A., et al. 2014, A&A, 563, A46
- Murphy, S. J., et al. 2015, MNRAS, 453, 2220
- Nardini, E., et al. 2015, Science, 347, 860
- Nazé, Y., et al. 2014b, A&A, 569, A70
- Nazé, Y., et al. 2014a, ApJS, 215, 10
- Nazé, Y., et al. 2015, MNRAS, 452, 2641
- Ofek, E. O., et al. 2013, ApJ, 768, 47
- Ofek, E. O., et al. 2014, ApJ, 781, 42
- Oskinova, L. M., et al. 2014, Nature Communications, 5, 4024
- Page, M. J., et al. 2012, MNRAS, 426, 903
- Parkin, E. R., et al. 2014, A&A, 570, A10
- Pierre, M., et al. 2016, A&A, in press
- Pillitteri, I., et al. 2014a, A&A, 567, L4
- Pillitteri, I., et al. 2014b, ApJ, 785, 145
- Pinto, C., et al. 2013, A&A, 551, A25
- Piro, L., et al. 2014, ApJ, 790, L15
- Ponti, G., et al. 2015, MNRAS, 453, 172

XMM-Newton Senior Review Proposal

Poppenhaeger, K., & Wolk, S. J. 2014, A&A, 565, L1
Read, A., et al. 2011, in The X-ray Universe 2011, ed. J.-U. Ness & M. Ehle, 135
Reis, R. C., et al. 2014, Nature, 507, 207
Remage Evans, N., et al. 2014, ApJ, 785, L25
Reyes-Iturbide, J., et al. 2014, AJ, 148, 102
Ricci, C., et al. 2014, A&A, 567, A142
Roberts, M. S. E., et al. 2015, arXiv:1502.07208
Robrade, J., et al. 2014, A&A, 561, A124
Romani, R. W. 2015, ApJL, 812, L24
Rosen, S. R., et al. 2015, arXiv:1504.07051
Sanz-Forcada, J., Stelzer, B., & Metcalfe, T. S. 2013, A&A, 553, L6
Sasaki, M., et al. 2014, A&A, 563, A9
Schulze, S., et al. 2014, A&A, 566, A102
Seitzzahl, I. R., 2015, MNRAS, 447, 1484
Snowden, S. L., et al. 2008, A&A, 478, 615
Snowden, S. L., et al. 2009, ApJ, 691, 372
Starling, R. L. C., et al. 2013, MNRAS, 431, 3159
Starling, R. 2015, in The Extremes of Black Hole Accretion, 112
Stelzer, B., et al. 2013, MNRAS, 431, 2063
Takey, A., et al. 2014, A&A, 564, A54
Tiengo, A., & Mereghetti, S. 2006, A&A, 449, 203
Toalá, J. A., et al. 2012, ApJ, 755, 77
Toalá, J. A., et al. 2014, AJ, 147, 30
Toalá, J. A., et al. 2015a, ApJ, 799, 67
Toalá, J. A., et al. 2015c, arXiv:1512.01000
Toalá, J. A., et al. 2015b, MNRAS, 446, 1083
Tofflemire, B. M. 2013, ApJ, 779, 22
Tombesi, F., et al. 2014, MNRAS, 443, 2154
Valencic, L. A., & Smith, R. K. 2013, ApJ, 770, 22
Valencic, L. A., & Smith, R. K. 2015, ApJ, 809, 66
Viganò, D., et al. 2013, MNRAS, 434, 123
Walsh, B. M., et al. 2014, Space Weather, 12, 387
Walton, D., et al. 2015a, ApJ, 799, 122
Walton, D., et al. 2015b, ApJ, 806, 65
Watson, D., et al. 2013, ApJ, 768, 23
Weng, S.-S., et al. 2015, ApJ, 805, 81
Wilcox, H., et al. 2015, MNRAS, 452, 1171
Zhang, N.-X., et al. 2014a, ApJ, 792, 58
Zhang, S., et al. 2014b, ApJ, 794, 61
Zhekov, S. A. 2014, MNRAS, 443, 12
Zoghbi, A., et al. 2012, MNRAS, 422, 129
Zoghbi, A., et al. 2014, ApJ, 789, 56

XMM-Newton Senior Review Proposal

Appendix B. Acronyms

3XMM-DR5.....	Serendipitous Source Catalog Data Release 5
ADAP.....	Astrophysics Data Analysis Program
ADS.....	Astrophysics Data Service
AGN.....	Active Galactic Nuclei
AO.....	Announcement of Opportunity
ARCHES.....	Astronomical Resource Cross-matching for High Energy Studies
ARK.....	Astrophysics Research Knowledgebase
ASB.....	Active Star Binaries
ASCA.....	Advanced Satellite for Cosmology and Astrophysics
<i>Astro-H</i>	<i>Astro-H X-ray Observatory</i>
<i>AstroSat</i>	<i>AstroSat Observatory</i>
AXP.....	Anomalous X-ray Pulsar
BLR.....	Broad Line Region
BROWSE.....	HEASARC mission data and parameter search tool
CalDB.....	Calibration Data Base
CCD.....	Charge-Coupled Device
CCF.....	Current Calibration Files
CCO.....	Compact Central Object
<i>Chandra</i>	<i>Chandra X-ray Observatory</i>
CHEERS.....	Chemical Enrichment RGS Cluster Sample
CIAO.....	<i>Chandra</i> Interactive Analysis of Observations package
CIE.....	Collisional ionization Equilibrium
Co-I.....	Co-Investigator
COR.....	Contracting Officer's Representative
COSMOS.....	Cosmological Evolution Survey
CT.....	Compton Thick
CTI.....	Charge Transfer Inefficiency
CU.....	Columbia University
CV.....	Cataclysmic Variable
CXB.....	Cosmic X-ray Background
DR5.....	Data Release 5
eeHIFLUGCS.....	Extremely Expand Highest X-ray FLUX Galaxy Cluster Sample
EPIC.....	European Photon Imaging Camera
ESA.....	European Space Agency
ESAC.....	European Space Astronomy Center
ESAS.....	<i>XMM-Newton</i> Extended Source Analysis Software
EW.....	Equivalent Width
EXTraS.....	Exploring the X-ray Transient and variable Sky
Fcov.....	Covering Factor
<i>Fermi</i>	<i>Fermi γ-Ray Observatory</i>
FITS.....	Flexible Image Transport System
FOV.....	Field of View
FTE.....	Full Time Equivalent
FTP.....	File Transfer Protocol
FUV.....	Far Ultra Violet
FWHM.....	Full Width at Half Maximum
GALEX.....	<i>Galaxy Evolution Explorer</i>
GO.....	Guest Observer
GOF.....	NASA/GSFC Guest Observer Facility
GPG.....	GNU Privacy Guard
GRB.....	Gamma Ray Burst
GSFC.....	Goddard Space Flight Center
HEASARC.....	High Energy Astrophysics Science Archive Research Center
HESS.....	High Energy Stereoscopic System

XMM-Newton Senior Review Proposal

HETG.....	High Energy Transmission Grating
HPD.....	Half Power Diameter
<i>HST</i>	Hubble Space Telescope
HVC.....	High Velocity Cloud
IACHEC.....	International Consortium for High-Energy Calibration
IGM.....	Intergalactic Medium
IMBH.....	Intermediate-Mass Black Hole
<i>INTEGRAL</i>	<i>International Gamma-Ray Astrophysics Laboratory</i>
IR.....	Infra Red
ISM.....	Interstellar Medium
IT.....	Information Technology
KEPLER.....	Kepler Observatory
LBV.....	Luminous Blue Variables
Λ CDM.....	Lambda Cold Dark Matter
LETG.....	Low Energy Transmission Grating
LMC.....	Large Magellanic Cloud
LMXB.....	Low Mass X-ray Binary
LP.....	Large Programs
LSS.....	Large Scale Structure Survey
MAST.....	Mikulsky Archive for Space Telescopes
MHD.....	Magneto Hydrodynamics
MIR.....	Mid IR
MO&DA.....	Mission Operations and Data Analysis
MOS.....	Metal Oxide Silicon X-ray Detector
MSP.....	Millisecond Pulsar
MW.....	Milky Way
NAS.....	National Academy of Sciences
NASA.....	National Aeronautics and Space Administration
NLS1.....	Narrow Line Seyfert 1
NS.....	Neutron Star
NTH.....	Equatorial Column Density
<i>NuSTAR</i>	<i>Nuclear Spectroscopic Telescope Array</i>
NUV.....	Near Ultra Violet
OM.....	Optical Monitor
OMCat.....	Optical Monitor Catalog
OM SUSS.....	Optical Monitor Source Survey
PI.....	Principal Investigator
PIMMS.....	Portable Interactive Multi-Mission Simulator
<i>Planck</i>	<i>An ESA microwave space observatory</i>
PMO.....	Primary Mission Objective
PN.....	PN style EPIC CCD detector
PNe.....	Planetary Nebulae
PSF.....	Point Spread Function
QPO.....	Quasi-Periodic Oscillation
RGA.....	Reflection Grating Array
RGS.....	Reflection Grating Spectrometer
<i>ROSAT</i>	<i>Rontgen Satellite</i>
RPS.....	Remote Proposal Submission
<i>RXTE</i>	<i>Rossi X-ray Time Explorer</i>
SAS.....	Science Analysis System
SDSS.....	Sloan Digital Sky Survey
SED.....	Spectral Energy Distribution
SGR.....	Soft Gamma-ray Repeater
SMBH.....	Supermassive Black Hole
SMC.....	Small Magellanic Cloud
SMD.....	Science Mission Directorate
S/N.....	Signal to Noise

XMM-Newton Senior Review Proposal

SNe.....	Supernovae
SNR.....	Supernova Remnant
SOC.....	Science Operations Center
SPI.....	Star Planet Interactions
<i>Spitzer</i>	<i>Spitzer Space Telescope</i>
SR.....	Senior Review
SRON	Netherlands Institute for Space Research
SSC	Serendipitous Source Catalog
SSSC.....	Slew Survey Source Catalog
SWCX.....	Solar Wind Charge Exchange
<i>Swift</i>	<i>Swift Gamma-Ray Burst Mission</i>
<i>Suzaku</i>	<i>Suzaku X-ray Telescope</i>
SXS.....	Soft X-ray Spectrometer
S-Z.....	Sunyaev-Zel'dovich
TDE.....	Tidal Disruption Event
ToO	Target of Opportunity
UFO	Ultra Fast Outflow
ULX.....	Ultra-Luminous X-ray source
US.....	United States
USNO	US Naval Observatory
UV.....	Ultra Violet
VLP	Very Large Program
WA.....	Warm Absorber
WHIM.....	Warm Hot Intercluster Medium
<i>XMM</i>	<i>XMM-Newton</i>
<i>XMM-ESAS</i>	<i>XMM-Newton Extended Source Analysis Software</i>
<i>XMM-Newton</i>	<i>Newton X-ray Multi-Mirror Observatory</i>
XRB	X-ray Binary
XSA.....	<i>XMM-Newton</i> Science Archive
XXL	Extra Extra Large

XMM-Newton Senior Review Proposal

Appendix C. Online Bibliography

The *XMM* bibliography of refereed papers (a GOF product) can be found at:
<http://heasarc.gsfc.nasa.gov/docs/xmm/xmmbib.html>

A list of Ph.D. theses using *XMM* data can found at:
https://heasarc.gsfc.nasa.gov/docs/xmm/phd_bibs_alpha.html